Rare Met. (2024) 43(7):2913–2939
https://doi.org/10.1007/s12598-024-02638-4

RARE METALS

REVIEW

Solar-driven photothermal catalytic CO_2 conversion: a review

Bachirou Guene Lougou, Bo-Xi Geng, Ru-Ming Pan, Wei Wang, Tian-Tian Yan, Fang-Hua Li, Hao Zhang, Oraléou Sangué Djandja, Yong Shuai*, Meisam Tabatabaei, Daniel Sabi Takou

Received: 20 April 2023 / Accepted: 21 August 2023 / Published online: 18 April 2024

Abstract It is highly desirable to seek green and sustainable technologies, such as employing photothermal effects to drive energy catalysis processes to address the high energy demand and associated environmental impacts induced by the current methods. The photothermocatalysis process is an emerging research area with great potential in efficiently converting solar energy through various catalytic reactions. However, achieving simultaneously high conversion efficiency, cyclability, and durability is still a daunting challenge. Thus, tremendous work is still needed to enhance solar photothermal catalytic conversion and promote its large-scale applications. This review developed the principles of coupling solar photon and thermal fields underlying the photothermal effect, exploration of efficient nanocatalysts, development of optofluidic reactor model, and photothermal synergistic-driven CO_2 reduction mechanisms. The ultimate goal was to provide an effective approach that can effectively convert solar energy into photocarriers/hot-electrons and heat, and importantly, can couple them to regulate catalysis reaction pathways toward the production of value-added fuel and chemical energy.

Keywords Photochemistry; Photothermal; CO_2 catalytic conversion; Nanomaterial; Solar fuels and chemicals

1 Introduction

Sunlight-powered catalytic conversion of CO_2 over earth-abundant metal-oxide materials [1–4] offers promising solutions to generate energy-rich fuels [5–8], which could

Bachirou Guene Lougou and Bo-Xi Geng contributed equally to this work.

B. G. Lougou B.-X. Geng, R.-M. Pan, W. Wang, T.-T. Yan, Y. Shuai*
School of Energy Science and Engineering, Harbin Institute of Technology, Harbin 150001, China
e-mail: shuaiyong@hit.edu.cn

B. G. Lougou
MIIT Key Laboratory of Critical Materials Technology for New Energy Conversion and Storage, Harbin Institute of Technology, Harbin 150001, China

F.-H. Li
State Key Laboratory of Urban Water Resource and Environment, Harbin Institute of Technology, Harbin 150090, China

H. Zhang
School of Electrical Engineering and Automation, Harbin Institute of Technology, Harbin 150001, China

O. S. Djandja
Guangdong Provincial Key Laboratory of Distributed Energy Systems, Engineering Research Center of None-Food Biomass Efficient Pyrolysis and Utilization Technology of Guangdong Higher Education Institutes, Dongguan University of Technology, Dongguan 523808, China

M. Tabatabaei
Higher Institution Centre of Excellence (HICoE), Institute of Tropical Aquaculture and Fisheries (AKUATROP), Universiti Malaysia Terengganu, 21030 Kuala Nerus, Malaysia

M. Tabatabaei
Department of Biomaterials, Saveetha Dental College, Saveetha Institute of Medical and Technical Sciences, Chennai 600 077, India

D. S. Takou
École Polytechnique d'Abomey-Calavi, University of Abomey-Calavi, 2009 Cotonou, Benin

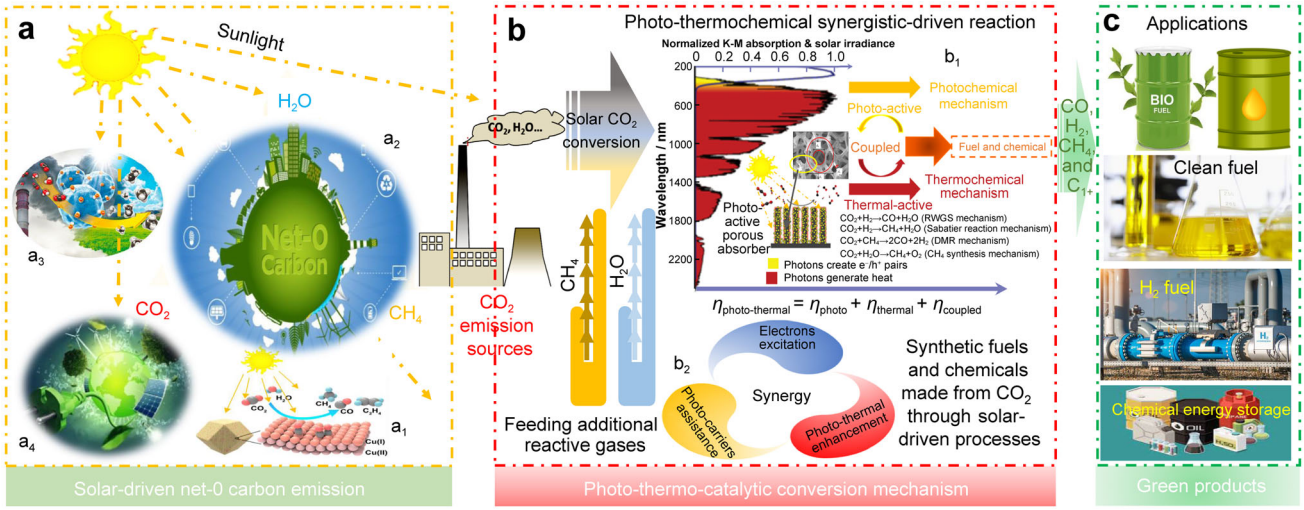

Fig. 1 Principles of coupling solar photon and thermal fields underlying photothermal effect, exploration of efficient nanocatalysts and their design strategies, development of optofluidic reactor model, and photothermal synergistic-driven CO_2 reduction by H_2, CH_4 and H_2O, with ultimate goals of providing an alternative approach for efficient sunlight conversion, solar fuel production, and high-density chemical energy storage: **a** efficient utilization of solar energy (**a1** reproduced with permission from Ref. [14]. Copyright 2021, American Chemical Society. **a3** Reproduced with permission from Ref. [15]. Copyright 2021, Elsevier). **b** Photothermochemical synergistic-driven reaction (**b1** reproduced with permission from Ref. [16]. Copyright 2016, American Chemical Society). **c** Applications of production gas

simultaneously alleviate energy shortage and environmental deterioration. A global investigation of possible CO_2 utilization into fuels reported a potential 50% emission reduction [9]. As shown in Fig. 1 [10–12], the synthetic natural gas (SNG), CO, and/or H_2 released from the solar-driven chemical catalytic decomposition of CO_2, H_2O and CH_4 can be a building block for synthesizing industrial combustible feedstock. Given its contribution to sustainable development, SNG serves as an attractive fuel due to its high gravimetric energy density and good compatibility with today's infrastructure. CO is another interesting chemical compound because it forms an important building block for the production of methanol and long-chain hydrocarbons. Reducing CO_2 into CO is also important regarding today's atmospheric concentrations of CO_2 [13–15]. The major challenge is the provision of hydrocarbon fuels with net-zero emissions [16], which aligns with the carbon neutrality goals. Although effective paths have been provided to improve the efficiency of solar energy utilization, the success of this approach relies on the efficient conversion and storage strategy of the incoming solar multi-spectral band radiative flux. Various thermal, photo-, and photothermal catalysis processes have been developed to promote solar fuel and chemical energy conversion, delivering different reactivity, selectivity, and stability upon solar spectral absorption and transmission. Sunlight plays a varied role in the material physical–chemical properties evolution, dividing the reaction mechanisms into photo-, electro-, and thermochemical. Depending on a specific catalyst system, tightly coupling electric field, radiation, and temperature, those mechanisms could work together, resulting in complex reaction conditions. The thermal process using conventional thermocatalysts is typically characterized by high temperature, active material sintering, big temperature swings, large heat loss, high thermodynamic constraints, and less than 10% solar fuel efficiency. In comparison, photocatalysis is characterized by low reaction rates and seriously suffers from the solar fuel efficiency that is still less than 5%. The main issues are associated with the weak absorption of sunlight in visible and infrared (IR) regions, very low apparent quantum efficiency, and rapid recombination of carriers. Plenty of studies have been developed on solar thermo- or photocatalytic process, but in neither case was the coupling of solar photon and thermal fields underlying the photothermal effect addressed in depth. Most current studies still cannot completely exclude or extract the influence of the photothermal synergistic effects. Regardless, developing a reliable and affordable renewable system for generating clean fuels and chemical energy through CO_2 photothermocatalytic conversion is a critical research focus for the low-carbon energy transition and rapid environment remediation.

Exploiting the photothermal effect by combining the advantages of solar photon and thermal fields has emerged as a new and fast-growing research area providing a straightforward and effective method for efficient solar spectrum utilization. However, the photothermal effect and synergistic mechanism between photons, hot carriers, and heat force-driven catalysis reactions under photothermal

multi-field coupling conditions have not been clear. This induces the inefficiency of the operation of existing systems and technics. Research and innovative ideas are still desired to enhance the optical and quantum efficiencies, spectral transfer and heat transmission efficiency, and kinetic of multiple electron transfer processes while preventing electron–hole recombination and accelerating light to thermal energy conversion. This cannot be separated from material engineering since the adequate arrangement of catalysts inside the reactor will be crucial for fully exploiting its full energy potential. Thus, it is imperative to work at different scales, from the architecture of nanocrystal superstructures to the macroscopic shaping of the catalyst and developing materials with an even better overall performance, possibly by enhancing the photoactivated contribution.

Regarding the current research trend, as shown in Fig. 1, the performance of solar energy storage systems might be boosted significantly by exploiting both light and heat compared to using only one energy source input, bringing down the high-energy penalty and low efficiency with accompanying CO_2/C footprint. Several fundamental challenges still exist, and much more effort must be devoted to achieving enhanced and efficient solar energy harnessing. Yet, there is a lack of fundamental mechanisms of solar-driven CO_2 catalytic reduction reactions and rational design of energy storage material that can efficiently exploit light to induce heating. The photoinduced charge separation and transfer are crucial for determining the activity under photothermal conditions, but most conventional characterizations could not provide sufficient information about these phenomena, which in turn seriously hinders the efficiency of green fuel production through a photodriven CO_2 conversion mechanism. Considerable research efforts must be devoted to developing novel materials with broad photoresponse to take full advantage of the solar spectrum. Still, it is hard to determine whether the reaction mechanism is light-driven or light-induced. However, it can be confirmed that the catalytic activity has been enhanced by the effect of light. Besides, there has been a lack of studies on reactors for photothermal processes despite abundant efforts devoted to advanced materials research. Thus, an in-depth understanding of the principles of coupling solar photo and thermal energy underlying the photothermal effect is needed to overcome serious impediments to scientific and technology progress in achieving high-efficiency, low-cost solar energy conversion and usage.

This review clarifies the state of the current research and the dynamics of photochemical technological development while also demonstrating photothermal effect-driven catalytic CO_2 conversion. Following thermodynamic principles, reaction mechanisms, and kinetics, the underlying methods and techniques, and photocatalysis resulting in a significant CO_2 conversion rate are provided to obtain insight into the design of advanced catalyst systems and innovations in reactor engineering. The scientific issues and key limiting factors associated with light-induced photocatalytic CO_2 conversion are also highlighted to indicate the means to upgrade a photochemical mechanism to more reasonable and highly efficient photothermal catalysis mainly characterized by photoactivated thermocatalysis, thermal-mediated photocatalysis, and photothermocatalysis driving forces. Next, this review describes a photothermocatalysis system that exploits ultraviolet–visible (UV–Vis) light combined with solar intensity. This system represents a significant breakthrough in achieving a low-energy input system and ultrahigh conversion efficiency. After addressing the key achievements in the field, this review also shares some key perspectives and insights concerning the path toward an effective solar-driven CO_2 catalytic conversion system.

2 CO_2 photocatalytic reduction

2.1 CO_2 photoreduction and performance evolution

A photochemical reaction is an artificial photosynthetic technology inspired by natural photosynthesis that can be applied to the light-induced chemical conversion of CO_2 into alternative fuels and derived chemicals [17–20]. The photodriven CO_2 reduction process can make full use of solar energy across several CO_2 reduction reaction (RR) pathways, such as reverse water–gas-shift reaction, Sabatier reaction, methanation reaction, MeOH synthesis reaction, and even C2+ hydrocarbon synthesis reaction [21]. Considering the reverse water–gas-shift (RWGS) reaction mechanism: $CO_2 + H_2 \xrightarrow[h\nu > 3.2\,eV]{M/TiO_2} CO + H_2O$, where M is a noble metal, and the intrinsic chemical reaction mechanism indicates that the reaction is initiated photothermally due to the thermal energy generated by the active catalyst under incident photons. However, thermally driven water–gas-shift reaction (WGSR) kinetics may result in a more complex reaction mechanism due to competitive CO and H_2O absorption relative to photon-driven kinetics, which fits well with the Langmuir–Hinshelwood kinetics [22]. As depicted in Fig. 1, other gas-phase reaction mechanisms, including $CO_2 + 2H_2O \rightarrow CH_4 + 2O_2$ and Sabatier reaction: $CO_2 + 4H_2 \rightarrow CH_4 + 2H_2O$ for CH_4 synthesis, dry reforming of methane (DRM): $CO_2 + CH_4 \rightarrow 2H_2 + 2CO$ for syngas production, and MeOH formation reactions such as $2CO_2 + 4H_2O \rightarrow$

$2MeOH + 3O_2$ and $CO_2 + 3H_2 \rightarrow MeOH + H_2O$ adapt well to the photodriven catalysis applications. However, how to efficiently construct and simultaneously optimize the optical and catalytic performances of the catalyst systems is the main challenge associated with CO_2 photodriven conversion processes [23, 24].

As depicted in Fig. 2a, tris(bipyridine)ruthenium (II) chloride hexahydrate ($[Ru(bpy)_3]Cl_2\ 6H_2O$) photosensitized ultrathin CoAl-layered double hydroxide (CoAl-LDH) has a photocatalyst activity, converting CO_2 into 43.73 $mmol{\cdot}g^{-1}{\cdot}h^{-1}$ of CO under visible light [17]. This demonstrates the high potential applicability of such a process in carbon-neutral energy conversion. The detailed reaction mechanism can be seen in Fig. 2b. The photosensitizer is a sacrificial material such as ruthenium-polypyridyl, porphyrin, and organic dyes with high photon-absorption potential in UV–Vis light and photocatalytic activity in the reacting media [25]. The visible light

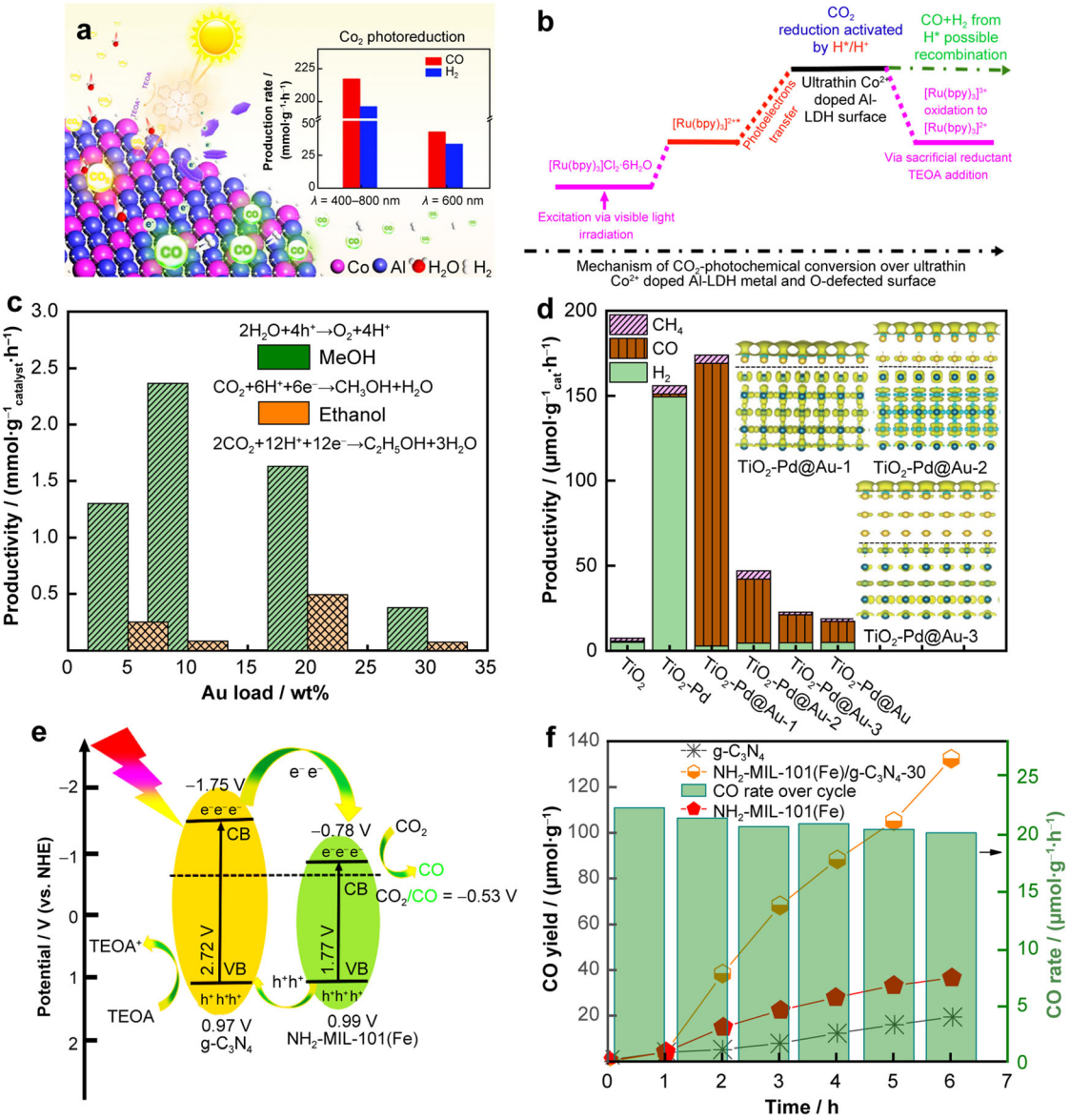

Fig. 2 **a, b** Solar irradiance-induced CO_2 catalytic reduction and photocatalyst activity: $Ru[(bpy)_3]Cl_2\ 6H_2O$ photosensitized u-CoAl-LDH photocatalytic CO_2 reduction at 400–800 and 600 nm. Reproduced with permission from Ref. [17]. Copyright 2020, American Chemical Society. **c** Au*x*@ZIF-67 enhanced photocatalyst activity for CO_2 photoreduction into MeOH and ethanol. Reproduced with permission from Ref. [27]. Copyright 2020, American Chemical Society. **d** TiO_2-Pd@Au*x* photocatalyst activity for H_2 and CO production and charge density with increase in Au thickness. Reproduced with permission from Ref. [28]. Copyright 2020, the Royal Society of Chemistry. **e**, **f** Synergetic activity of g-C_3N_4 and NH_2-MIL-101(Fe) for CO_2 photocatalytic reduction under $\lambda > 420$-nm visible light. Reproduced with permission from Ref. [32]. Copyright 2020, American Chemical Society

absorption is attributed to the depth of the absorber bandgap, in which the smaller the catalyst bandgap is and the stronger the interaction with CO_2 and H_2O is, the higher the photocatalyst CO_2-splitting activity under visible light is. The higher photocatalyst activity could be attributed to charge separation, efficient charge transfer, or reactive flow access to the active sites on the catalyst's surface. Considering the CO_2 photocatalytic reduction mechanism, CO_2 activation across surface-modified semiconductors can be improved by controlling the electrons and protons transfer [26]. However, compared to the heterojunction-type, the Z-scheme structure is employed as a photocatalytic system for enabling high charge-separation efficiency as well as strong redox ability. As shown in Fig. 2c, the loading of plasmonic Au nanoparticles into the zeolitic imidazolate framework (ZIF-67) was found to improve the activity and stability of the Co photocatalyst for CO_2 reduction with MeOH and ethanol productivity by up to 2.5 and 0.5 $mmol{\cdot}g^{-1}{\cdot}h^{-1}$, respectively [27]. As with the mechanism described in Fig. 2b, CO_2 reduction is activated by the accumulated photoinduced energetic electrons, including hot and excited electrons at the catalyst's surface. The activated CO_2 undergoes a photochemical transformation concerning the active site's behavior in terms of the Lewis acid or base formed by the metal cation clusters. Au and Pd co-catalyze the synergetic effects of increasing surface catalyst activity and energetic charge transfer at the interface of TiO_2, thereby resulting in efficient CO_2 photoreduction with 166.3 $\mu mol{\cdot}g^{-1}{}_{cat}{\cdot}h^{-1}$ CO productivity [28].

Nanocomposite material synthesis, such as TiO_2-Pd@Au photocatalyst system, is used as a strategy to tune the catalyst activity of TiO_2 [29] for H_2 and CO selectivity from TiO_2-Pd and TiO_2-Au photocatalyst activity toward H_2O- and CO_2-splitting, respectively, as shown in Fig. 2d. The thickness of the Au catalyst is the determining factor for increasing CO selectivity, with a maximum production rate using TiO_2-Pd@Au with 4.5-mg TiO_2-Pd used for the synthesis (TiO_2-Pd@Au-1). Generally, the thinner the Au nanoparticles are, the better the CO_2-splitting catalytic activity is [28]. Recently, Li et al. [30] highlighted the synthesis strategy and CO_2 photoreduction mechanisms of 1D copper-based heterostructures, demonstrating the photoactivity and photostability enhancement of copper-based oxide-supported co-catalyst systems. The visible light-induced CO_2 photocatalytic reduction with TiO_2 is enhanced by ionic liquid (IL = $[P4444]_3$[p-2,6-O-4-COO] and $[N4444]_3$[p-2,6-O-4-COO]) with a high affinity of binding CO_2 into a promoter IL-CO_2 complex solution that serves as a photosensitizer for subsequent CO_2 conversion into 3.52 $\mu mol{\cdot}g^{-1}{\cdot}h^{-1}$ CH_4 [31]. IL $[P4444]_3$[p-2,6-O-4-COO] has a higher CO_2 capture and absorption potential. Its enhanced effects for CO_2 photo-reduction are attributed to its capacity to activate and bind CO_2 with active photocatalysts by forming a photosensitizer. Considering the photocatalyst activity of the amino-functionalized Fe-based Materials Institute Lavoisier (MIL) NH_2-MIL-101(Fe) and the sole g-C_3N_4, Dao et al. [32] synthesized a novel catalyst NH_2-MIL-101(Fe)/g-C_3N_4 that produced 132.8 $\mu mol{\cdot}g^{-1}$ CO, 6.9 times and 3.6 times higher than g-C_3N_4 and NH_2-MIL-101(Fe), respectively. As depicted in Fig. 2e, f, the higher catalyst activity of NH_2-MIL-101(Fe)/g-C_3N_4 can be attributed to CO_2 and visible light absorptivity by the -NH_2, the high porosity of the main material, and the subsequent CO_2 reduction via a gas–solid interface in a solvent-freereaction.

The catalyst activity in terms of efficient light absorptivity, CO_2 fixation, effective charge separation, and active site accessibility of g-C_3N_4 can be improved, resulting in a threefold CO yield by substituting α-Fe_2O_3 dendritic patterns to g-C_3N_4 [33]. Further, Tahir [34] reported an 18-fold higher photocatalytic activity of H_2 and a sixfold higher yield of CO, with H_2 and CO production rates of 91.9 and 4.97 $mmol{\cdot}g^{-1}{}_{cat}{\cdot}h^{-1}$, respectively, using a protonated graphitic carbon nitride (pg-C_3N_4)/Ti_3AlC_2/TiO_2 complex catalyst system. By using a g-C_3N_4/CdS composite photocatalyst, Vu et al. [35] found that triethanolamine (TEOA) and $[Co(bpy)_3]^{2+}$ are the main factors activating the catalyst toward CO and H_2 formation with 234.6 $\mu mol{\cdot}g^{-1}{\cdot}h^{-1}$ of CO yield, that is, 25.5-fold higher than pristine g-C_3N_4. Considering the reaction mechanism and modified g-C_3N_4 catalyst activity, the literature has focused on the enhanced photocatalyst activity of g-C_3N_4 as associated with g-C_3N_4 hybridity and multiheterojunction within the sample [36–38].

High H_2 selectivity may be associated with higher photocatalytic activity toward H^+ and electron generation/transfer following the breakage of C-O or O-H bonds and C-H or H-OCH_3 bond formation flexibility and efficiency [39, 40]. H_2 selectivity at the TiO_2 catalyst surface is outperformed, up to 880 $\mu mol{\cdot}h^{-1}{\cdot}g^{-1}$ using TiO_2/rGO-Mo_2C or 5.5 times the TiO_2/rGO activity [41]. For the newly reported CH_4 yield of 277 $mmol{\cdot}h^{-1}{\cdot}g^{-1}$ over ultrathin Mg–Al LDHs matrix and Ru nanoparticles (Ru@FL-LDHs) [42], the photocatalysts contained layered double hydroxides resulting in significant CO_2 photoreduction due to the concentration of -OH in the chemically reacting media.

The CO_2 conversion reaction pathway could follow CO, CH_4 and CH_3OH formation through the photoreduction mechanism depending on the number of electrons and protons participating in the chemical reaction. The formation of CH_4 may prevail over the other products, demonstrating CO_2 methanation as the most effective CO_2 photocatalytic reduction process. Nonetheless, selectivity for CO_2 photoreduction can be controlled through the reaction mechanism and pathways, which are still not

Table 1 CO_2 photochemical conversion performance evaluation: high-performance photocatalyst materials, including a photosensitizer and other scarifying agents, resulting in effective fuel yields such as CO, H_2, MeOH and CH_4 being highlighted to provide new insight into advanced photocatalyst design for improving CO_2 conversion through solar photo component

Operating conditions	Fuels yield	Photocatalyst materials	Refs.
300-W Xe lamp: 400–800-nm irradiation, 500 $mW{\cdot}cm^{-2}$, L = 11 cm; 0.18 MPa CO_2	218.13 $mmol{\cdot}g^{-1}{\cdot}h^{-1}$ CO at 600 nm irradiation	$Ru[(bpy)_3]Cl_2.6H_2O$ photosensitizer; u-CoAl-LDH	[17]
Abet 103; 150 $mW{\cdot}cm^{-2}$ light intensity	6490 $\mu mol{\cdot}g^{-1}$ MeOH; 1980 $\mu mol{\cdot}g^{-1}$ ethanol	Au_{20}@ZIF-67 with 10 wt% TEOA	[27]
315–600 nm; 380 $W{\cdot}m^{-2}$; CO_2:H_2O = 30:1 molar ratio; 0.31 $ml{\cdot}min^{-1}$ gas flow rate	0.191 $\mu mol{\cdot}h^{-1}{\cdot}g^{-1}$ CH_4; 0.111 $\mu mol{\cdot}h^{-1}{\cdot}g^{-1}$ of CO	N-doped TiO_2	[45]
300-W Xe lamp, 2.7 $mW{\cdot}cm^{-2}$; T = 160 °C; $420 < \lambda < 780$ nm; 0.15 MPa CO_2	166.3 $\mu mol{\cdot}h^{-1}{\cdot}g^{-1}$ CO yield	TiO_2-Pd@Au core–shell	[28]
$\lambda > 420$ nm; 0.4 g TiO_2; 0.5 $mol{\cdot}L^{-1}$ of IL; 0.1 g CO_2	3.52 $\mu mol{\cdot}g^{-1}{\cdot}h^{-1}$ CH_4	TiO_2-$[P4444]_3$[gp-2,6-O-4-COO]	[31]
Photoluminescence spectroscopy λ_{ex} = 380 nm	132.8 $\mu mol{\cdot}g^{-1}$ CO yield	NH_2-MIL-101(Fe)/g-C_3N_4–30 wt%	[32]
300-W Xe lamp irradiation	566.4 $\mu mol{\cdot}g^{-1}$ CO	$Bi_{12}O_{17}Br_2$ nanotubes	[46]
Flue gas without water vapor at 20 °C	0.64 $mmol{\cdot}h^{-1}{\cdot}g_{MOF}{}^{-1}$ $HCOO^-$	$Ni_{0.75}Mg_{0.25}$-MOF-74; $[Ru(bpy)_3]Cl_2$ photosensitizer	[47]
Visible light; room temperature; normal pressure to 4.053 MPa	63.1 $mmol{\cdot}g^{-1}{\cdot}h^{-1}$ up to 736.3 $mmol{\cdot}g^{-1}{\cdot}h^{-1}$ HCOOH	Pt/In_2O_3/g-C_3N_4	[48]
Simulated sunlight; aqueous medium	3.95 $\mu mol{\cdot}g^{-1}{\cdot}h^{-1}$ CO, 1.50 $\mu mol{\cdot}g^{-1}{\cdot}h^{-1}$ CH_4, and 4.19 $\mu mol{\cdot}g^{-1}{\cdot}h^{-1}$ H_2	rGO-MoS_2/PPy-150	[49]
Visible irradiation $\lambda > 495$ nm; CO_2 atmosphere; electron donor BIH (0.1 $mol{\cdot}L^{-1}$)	38.5 ± 0.6 μmol CO yield; 427.4 μmol CO turnover number	fac-Re(bpy)$(CO)_3$Cl- Ru-$(bpy)_3{}^{2+}$-Nf	[50]
$\lambda > 495$ nm; 25 °C; 0.101325 MPa; 10-ml triethanolamine; 10-ml H_2O; 30-ml acetonitrile	78.1 $\mu mol{\cdot}g^{-1}$ CH_4 and 46.0 $\mu mol{\cdot}g^{-1}$ CO over 10 h	Covalent triazine framework and black phosphorus (CTF-BP)	[51]
Visible light illumination LED-405 nm; $NaHCO_3$ solution	173.7 $\mu mol{\cdot}g^{-1}{\cdot}h^{-1}$ H_2; 105 $\mu mol{\cdot}g^{-1}{\cdot}h^{-1}$ CO	Cu-Pt/TiO_2-CuO	[52]
Under white LED λ = 780–850 nm; 26 °C; 40 $ml{\cdot}min^{-1}$ CO_2; 1 $\mu mol{\cdot}CoCl_2$; 15-mg 2,2-bipyridine; 3-ml 10%TOA/ acetonitrile; 0.5-ml H_2O	209.24 $\mu mol{\cdot}g^{-1}{\cdot}h^{-1}$ CO	Polymeric carbon nitride-grafted hydroxyethyl groups (HCNT-NA)	[53]
300-W xenon lamp; λ = 385, 420 or 520 nm; room temperature	17.8 $\mu mol{\cdot}g^{-1}{\cdot}h^{-1}$ CO	g-C_3N_4/α-Fe_2O_3	[33]
UV light, I = 150 $mW{\cdot}cm^{-2}$	91.9 $mmol{\cdot}g^{-1}{}_{cat}{\cdot}h^{-1}$ H_2; 4.97 $mmol{\cdot}g^{-1}{}_{cat}{\cdot}h^{-1}$ CO	pg-C_3N_4/Ti_3AlC_2/TiO_2	[34]
150-W xenon lamp, $259 < \lambda < 1904$ nm; MeCN/ H_2O = 14:1; 0.5 g TEOA	234.6 $\mu mol{\cdot}g^{-1}{\cdot}h^{-1}$ CO	4 $\mu mol{\cdot}[Co(bpy)_3]Cl_2$; g-$C_3N_4$/CdS	[35]
500-W Hg high-pressure lamp, $\lambda > 400$ nm; 217 $mW{\cdot}cm^{-2}$ 0.4 MPa; T = 386 K	118 $\mu mol{\cdot}g^{-1}{\cdot}h^{-1}$ CO	CdS/ZnO	[54]
UV–Vis spectra	121 $\mu mol{\cdot}g^{-1}{\cdot}h^{-1}$ CH_4; 41 $\mu mol{\cdot}g^{-1}{\cdot}h^{-1}$ CH_3OH	α-Fe_2O_3/MoS_2	[37]
White light of 350–700 nm and ~234 $mW{\cdot}cm^{-2}$ of flux; ambient conditions; 70-ml CO_2; 4-ml H_2O(g)	CO_2 to 1081 $\mu l{\cdot}h^{-1}{\cdot}g^{-1}$ CH_4	Cu-1%-doped TiO_2 without sacrificial agent	[55]
Xenon light: 1600 W, AM1.5 G; 350–1000 nm; 1-ml H_2O; 3-ml MeCN; 1-ml TEOA; CO_2	2676.3 $\mu mol{\cdot}g^{-1}{\cdot}h^{-1}$ H_2 and 959.1 $\mu mol{\cdot}g^{-1}{\cdot}h^{-1}$ CO	Dibenzo[b,d]thiophene sulfone photocatalyst with a hole-scavenger sacrificial agent	[56]
300-W Xe lamp, λ = 420 nm; P_{CO2} = 0.101325 MPa	7368.7 $\mu mol{\cdot}g^{-1}{\cdot}h^{-1}$ CO	g-C_3N_4/$ZnIn_2S_4$	[57]
300-W Xe lamp, $\lambda \geq 420$ nm; 0.3 vol% of acetonitrile/ water	148.9 $\mu mol{\cdot}g^{-1}{\cdot}h^{-1}$ CO	$CsPbBr_3$ NCs/g-C_3N_4	[58]

Table 1 continued

Operating conditions	Fuels yield	Photocatalyst materials	Refs.
20 W of halogen lamps, 8-W·m^{-2} irradiance intensity; λ = 210 nm 25 °C	62.33 μmol·g^{-1}·h^{-1} H_2 and 907 μmol·g^{-1}·h^{-1} HCOOH	ZnO/CuO-$NaAlSiO_4$ (zeolitic framework)	[59]

clearly understood due to the lack of experimental insights regarding the directions of charge transfer and dynamics in the reacting media. Li et al. [43] demonstrated that nitrogen-doped carbon quantum dots (NCQDs) could significantly improve CO_2 photoreduction to CO, resulting in 84% selectivity, which could be ascribed to the efficient photon switching properties of the NCQDs. To promote the design of dual-functional catalysts and CO_2 utilization, Qi et al. [44] developed a bifunctional zero-dimensional cadmium sulfide quantum dots-two-dimensional titanium dioxide nanosheets (CdS/TNS) composite, allowing efficient CO formation and C–C coupled product selectivity through a cooperative reaction system catalyzed by benzyl alcohol. The cycling performance of CO_2 photoredox and the final achievable efficiency are still affected by the photoreduction thermodynamics, sluggish oxidative reaction kinetics, and other influencing factors. Furthermore, Table 1 [17, 27, 28, 31–35, 37, 45–59] summarizes the CO_2 photochemical conversion performance under different operating conditions and photocatalyst materials.

2.2 Photoreduction thermodynamics and influencing factors

2.2.1 *Photoreduction thermodynamics*

The tensile strain of the active atomic surface of the photocatalyst material has favorable effects on CO_2 binding and activation for subsequent CO_2 reduction, hot-electron transfer and charge separation, CO release, chemical stability, and energy barrier related to the low rate-limiting stage [46, 60, 61]. By considering the tensile strain of $Bi_{12}O_{17}Br_2$ nanotubes, Di et al. [46] reported a 14.4-fold greater CO_2 reduction, with CO productivity up to 34.5 μmol·g^{-1}·h^{-1}. As shown in Fig. 3a, increasing the temperature to 5–30 °C resulted in the raise of CO productivity from 28.3 to 34.5 μmol·g^{-1}·h^{-1}. By using a CdS/ZnO photocatalyst, Zhang et al. [54] obtained higher CO formation up to 118 μmol·g^{-1}·h^{-1} when the reaction temperature was increased to 386 °C. From a thermodynamic prospective, the role of tensile strain is to regulate the endergonic gap in favor of CO_2 activation and lower the energy barrier related to the rate-limiting step. Additionally, bimetallic Ni/Mg metal–organic frameworks (MOF) $Ni_{0.75}Mg_{0.25}$-MOF-74 could exhibit high photocatalyst activity for converting CO_2 from industrial flue gas into 0.64 mmol·h^{-1}·g^{-1} MOF $HCOO^-$ at 20 °C [47]. The strongest photocatalyst activity of MOF can be attributed to the Mg active sites for binding CO_2 and the synergetic photocatalyst activity of Mg and Ni stabilization [*OCOH] during CO_2 photoreduction. The mechanism and cycling performance of Ni-Mg bimetallic photocatalyst activity for CO and HCOOH formation at the interface of MOF-74 can be seen in Fig. 3b. While the synergistic effect between two metal components exhibits excellent catalytic performance in CO_2 photoredox processes, the design of efficient bimetallic catalyst and its CO_2 catalytic conversion mechanism remains a challenge [62].

The photocatalyst activity of a multi-functional catalyst consisting of $Pt/In_2O_3/g\text{-}C_3N_4$, in which $g\text{-}C_3N_4$-combined Pt co-catalyst activity induces H_2O conversion into H_2 and CO_2 bending by In_2O_3, results in 63.1 and 736.3 mmol·g^{-1}·h^{-1} of HCOOH formation at 0.10 and 4.05 MPa, respectively [48]. This catalyst is still considered a black box. However, Hu et al. [63] demonstrated its electronic structure and atomic coordination dynamic evolution in CO_2-splitting reactions by tracking the mechanism of the CO_2 photocatalyst pathway over the $[Ni(tpy)]^0$ sites. The NiH^- photocatalyst activity shifts the CO_2 photoreduction thermodynamic toward the formation of CO relative to that of CuH^-, which results in greater $HCOO^-$ selectivity [64]. Jones [65] recently found that MOFs with transition metals in the first row, namely, $Rb_{0.33}WO_3$ and TiO_2-MnO_x-Pt, were advanced photocatalysts with superior catalyst activity for CO_2 photoreduction into CO, CH_4 and CH_3OH under visible light. Following the CO_2-splitting photocatalytic activity of CuO, TiO_2 and Pt/TiO_2, a complex Cu-Pt/TiO_2-CuO catalyst system was proposed as a strategy for improving the synthesis of photocatalyst material to a point where it could yield 105 μmol·g^{-1}·h^{-1} CO [52]. The light absorption behavior of TiO_2 and CO_2 photocatalytic conversion in the visible region could increase, resulting in 1081 μl·h^{-1}·g^{-1} CH_4 yield by doping with Cu-1 at% [55]. CO_2 to CH_4 photoreduction is likely more thermodynamically favorable than CO formation from CH_4, yielding potential $E_0(CH_4) = -0.24$ V (vs. normal hydrogen electrode (NHE)) against $< E_0(CO) = -0.53$ V (vs. NHE) [51]. A recent study showed an endothermic character in CO_2 photoreduction of over 1.55 and 1.72 eV-energy barriers following exothermic formaldehyde and formic acid formation under 61.12 and 359.90 kJ·mol^{-1} enthalpy changes, respectively [66].

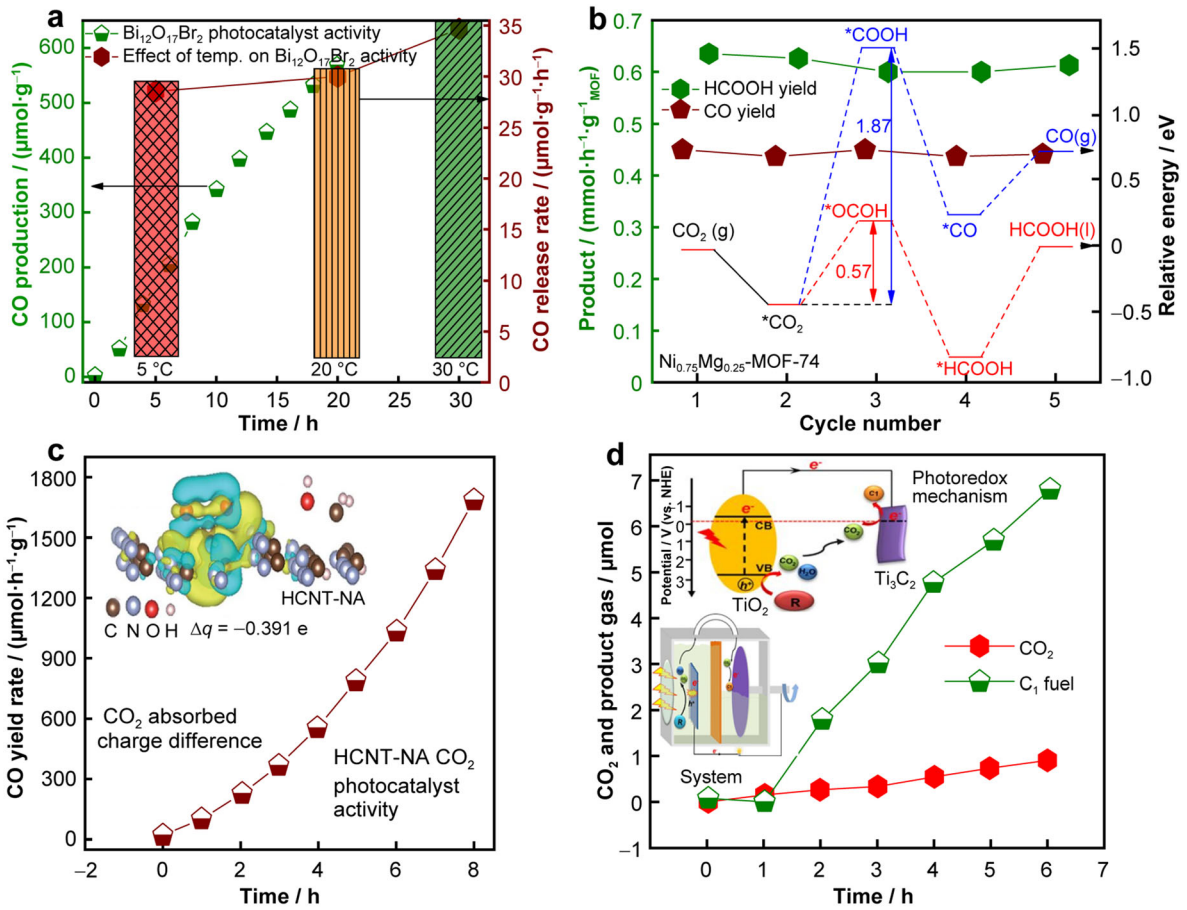

Fig. 3 **a** Photocatalyst activity for CO_2 photoreduction under visible light in $Bi_{12}O_{17}Br_2$ nanotubes. Reproduced with permission from Ref. [46]. Copyright 2020, American Chemical Society. **b** Ni0.75$Mg_{0.25}$-MOF-74 CO_2 photoreduction mechanism and photocatalyst activity toward CO and format productions. Reproduced with permission from Ref. [47]. Copyright 2020, the Royal Society of Chemistry. **c** CO_2-absorbed charge difference and polymeric carbon nitride-grafted hydroxyethyl groups catalyst activity toward CO formation. Reproduced with permission from Ref. [53]. Copyright 2020, the Royal Society of Chemistry. **d** Photochemical-integrated conventional electrochemical system and photoredox mechanism. Reproduced with permission from Ref. [71]. Copyright 2020, American Chemical Society

The CO_2 photoredox cycle, as well as the final achievable efficiency, is significantly affected by many issues, including tough CO_2 activation on active surfaces, sluggish oxidative half-reaction kinetics, undesired by-products, and poor stability. These issues could be avoided by developing cooperative photoredox systems exploring electron–hole pairs simultaneously. The cooperative photoredox reaction systems based on heterogeneous photocatalysis and the underlying reaction mechanisms have been highlighted by Yuan et al. [67], who provided a promising strategy for achieving efficient CO_2 re-use with alternative chemical production. Also, employing nanometal co-catalysts could significantly alleviate the issues associated with photoreduction half-reactions [68]. Among the underlying issues, the oxidative half-reaction for CO_2 photoreduction, the most crucial aspect for consideration, has been less investigated to date [69].

2.2.2 *Photoreduction-influencing factors*

The enhancing factors of TiO_2 photoreduction activity are largely attributed to the bandgap reduction (3.24–2.81 eV) due to the modification of electronic and structural properties induced by TiO_2, the presence of Cu^{1+}, and O-vacancies on the reacting surface. Recently, metal-free coupling covalent triazine framework/black phosphorus has been suggested to be an efficient and highly active catalyst for CO_2 photoreduction under visible light [51]. Efficient CO_2 photoreduction relies on an appropriate medium that facilitates photoinduced light absorption and highly promotes hot-electron or charge transfer and higher CO_2 binding behavior [49]. The design of advanced photosensitizers, for instance, the ternary system consisting of Nf polymer serving as a platform, Ru-$(bpy)_3^{2+}$ used as a conventional light absorber, and fac-Re(bpy)$(CO)_3$Cl

employed as a catalyst, could result in higher CO_2 photoreduction thermodynamic improvement in terms of photoconversion and photostability. Lee et al. [50] noted that the higher CO_2 photoreduction efficiency of fac-Re(bpy)$(CO)_3Cl^-$ Ru-$(bpy)_3^{2+}$-Nf can be attributed to the presence of Nf polymer that enhances the interaction between the exchange sites of sulfonic ionic and Ru-$(bpy)_3^{2+}$. An Nf membrane was also used in the photoreactor developed by Li et al. [70] to facilitate H^+ ion transport and (Fe^{2+}/Fe^{3+}) electron mediator exchanges through the twin reactor. For the first time, Zhang et al. [71] introduced a photochemical mechanism to the conventional electrochemical system that efficiently reduces CO_2 from wastewater into C1 + fuel with a 6.7 $\mu mol \cdot g^{-1} \cdot h^{-1}$ production rate, as shown in Fig. 3d. To overcome the difficulties related to lower C=O bond breakage energy and increase the surface accessibility of the photocatalyst, a catalyst system of polymeric carbon nitride-grafted hydroxyethyl groups can be used, which could result in 209.24 $\mu mol \cdot h^{-1} \cdot g^{-1}$ CO productivity as depicted in Fig. 3c [53].

In computational analyses, the mass transfer might be increased by raising the temperature and pressure, leading to an increase in product yield [72, 73]. A modified Stuchebrukhov–Hammes–Schiffer theory, combined with the Georgievskii–Stuchebrukhova theory [74], can be employed to analyze photocatalysis kinetic parameters, where proton–electron coupled transfer should occur at the surface of TiO_2 during CH_2-OH photoreduction. Regarding research on CO_2-splitting photocatalytic activity, the intrinsic mechanisms and kinetics of CO_2 photoreduction in terms of photoreactor configuration, photoredox thermodynamics, and spectral coupling of hot-electrons–proton transfer behavior throughout the catalyst micropores in the reactor are underexplored research topics [15, 75–78]. In terms of advanced photocatalyst material design to overcome the photoredox thermodynamics, modifying g-C_3N_4 into a Cring-C_3N_4 catalyst [79] could exhibit a 26-fold greater photocatalyst activity and a 24-fold faster CO_2 to CH_4 photogeneration rate. The Cring-C_3N_4 catalyst design is an advanced approach to upgrade the catalyst activity of g-C_3N_4 toward higher reactive species in terms of catalytic conversion and product selectivity. The enhancing indicators of the Cring-C_3N_4 photocatalyst are high-density electron transfer (eight electrons) and the extension of the carrier's lifetime and diffusion length due to the transition of the carbon-ring to the tri-s-triazine ring.

The restrictions on visible light absorption due to the poor active catalyst sites and the slow-moving charge separation related to $BiVO_4$ nanosheets (BVNS) and $BiVO_4$ in CO_2 photoreduction at the Z-scheme charge transfer interface were significantly improved, up to 9- and 35-fold, respectively, by modifying the pristine material into CuPc/Au-BVNS [80]. Similar improvements were also reported with the Z-scheme In_2S_3/WO_3 photocatalyst [81], indicating the pertinent effect of the catalyst system and composition. Further, the photocatalytic activity could be improved by adopting a single-atom catalyst design approach. For instance, the single-atom Fe active site design approach in the $Bi_4O_5I_2$-Fe30 catalyst system improves the insufficient electron–hole carrier separation, thereby boosting CO_2 photocatalytic reduction to 23.77 and 4.98 $\mu mol \cdot g^{-1} \cdot h^{-1}$ of CO and CH_4, respectively [82]. The single-atom Fe photoactivity performance indicator is strongly related to C-O bond dissociation in a COOH* intermediate subjected to a CO_2-photoreduction rate-limiting step [83]. Appropriate exploitation of the photocatalytic activity of Cu^+ sites [84] on light-irradiated CuO_X@p-ZnO catalysts could overcome the issues associated with multi-electron transfer and sluggish kinetic barriers. This approach can suppress the competing reaction restricting C–C bond formation regarding efficient CO_2 to C2+ conversion [10]. Furthermore, modifying In_2S_4 composition with Zn could potentially ameliorate CO_2-splitting photocatalytic activity, resulting in 7368.7 $\mu mol \cdot g^{-1} \cdot h^{-1}$ CO formation on the g-C_3N_4 surface [57] and 4261 $mmol \cdot g^{-1} \cdot h^{-1}$ of H_2 yield on the Co_3S_4 surface [85]. The higher performance of fuel yield can be attributed to the enhancement of electron–hole pair separation, transfer, and recombination of two interface materials.

3 CO_2 reduction through photoinduced hot-electron-thermal synergistic effects

3.1 CO_2 photothermocatalytic conversion mechanism

Solar spectral and heat-coupled effects were found to be suitable as alternative means of overcoming high-temperature thermodynamic limitations, large energy consumption, low catalyst activity, and hot-electron transport constrained by a high-potential chemical barrier, as well as low solar fuel and low chemical energy conversion efficiency [86–93]. The exploitation of the solar photonic components and intensity-synergistic CO_2-splitting and associated reactive gas chemical transformation characteristics is attracting researchers in search of the possibility of converting a full solar spectrum and increasing the solar-to-fuel efficiency. Still, the theoretical efficiency of solar fuel conversion is low at ~ 20% according to thermodynamic analyses and ~ 17% of the target attainable photoconversion efficiency over a 2- or 2.4-eV optimal bandgap [91]. Bhatta et al. [86, 94] recently developed a solar reactor that could use an integrated photothermal

process with catalyst materials that had photothermal properties that exhibited higher fuel yield, showing an increase of up to 8000 μmol·h^{-1} due to the combined effect of increasing temperature and photon flux. The underlying intrinsic mechanism of the directly irradiated reactor accounts for H_2O-assisted CO_2 photoreduction over a photothermal catalyst through a complex coupling of photolytic mechanisms, fluid flow motions, heat and mass transfers, and radiative flux transport mechanisms. The challenge lies in the synergetic effects of photoinduced light/thermal and its underlying conversion mechanisms and thermodynamics in the chemical reaction media [95–99].

The physical mechanism underpinning solar spectrum conversion consists of the direct absorption of photons from visible light and ultraviolet for the creation of e^-/h^+ and the activation of photochemical reaction, as well as the conversion of the remaining irradiance (visible and IR) into heat for the thermochemical process [16, 100]. This basic understanding of the mechanism of the in-situ sunlight distribution can provide insight into the selection and design of energy storage materials, accounting for both thermal and photocatalytic properties. The gas–solid thermal conversion of CO_2 is characterized by a complex mechanism, and the need to consider the pre-exponential factor is strongly related to the fact that the kinetics of CO_2-splitting is associated with the rate of CO yield [101–104]. As represented in Fig. 4a [17, 101], Fu et al. [101] demonstrated that CO formation from CO_2-splitting on a $LaMnO_3$(010) O-defected surface could be characterized by one transition state activating CO_2 decomposition, followed by CO desorption on the O-filled vacancy site. The final CO yield can be clearly attributed to the material composition and chemical activity of the surface because CO_2-splitting is highly pronounced at the irradiated active surface. Based on the photothermal principles depicted in Fig. 4a and b, the surface exposed to UV–Vis light would result in significant photocatalytic activity, while the absorbed radiant energy flux would generate heat by inducing thermal catalytic effects. The synergistic activity may be beneficial or result in competition reactions, depending on the physicochemical properties of the active material.

3.1.1 *Plasmon resonance excitation enhancing photothermal synergistic activity*

The in-situ microheat generation behavior of certain catalysts may contribute to the increase in the local reaction temperature by resulting in photothermal effects with complex reaction kinetics consisting of photodriven kinetic and additional thermal-driven kinetic. Regarding CO_2 catalytic conversion, the photothermal reaction rate is not dependent on the UV plasmon excitation of active catalysts or the generation of electron–hole pairs by the support [105, 106]. Instead, CO_2 binding and catalytic conversion were found to be pronounced by nonradiative relaxation of the active catalysts, followed by optical excitation of intra-/interband electrons, which is different from that of the photocatalytic conversion mechanism [90, 107]. Analyses of the thermal characteristics of Cu and Ni catalysts in Cu@Ni@ZIF-8 photothermal catalysts [108] have found that catalysts with higher in-situ heating properties result in significant promoting effects on the photocatalytic reaction rate. According to the literature, an effective method for whole range of solar spectrum utilization is shown in Fig. 4b [109], and the photothermocatalytic CO_2 conversion performance is strongly associated with the catalyst's visible light and ultraviolet absorption capacity. As indicated in the photochemical section, CO_2 binding on the catalyst is highly promoted by light irradiation, which facilitates H_2 dissociation into a short-lived Au-H due to hot-electrons transferred from the Au catalyst. Then, the fixed CO_2 and the intermediate Au-H formed undergo photothermal reduction into CO. As indicated in Fig. 4c, Au's higher visible light absorption and plasmon resonance ability [99] enhance the CO_2 photothermal catalytic reduction over Au/CeO_2 to reach up to 10 times greater than the thermal process [2]. The synergistic photothermal activity is greatly improved by coupling plasmon resonance excitation on the $Ag/W_{18}O_{49}$ catalyst [8]. Further, the CO_2 photothermocatalytic reduction over m-WO_{3-x} is highly improved due to the catalyst's higher lattice O_2 mobility, which facilitates the photoinduced electron transfer toward C/CO formation and CH_4 selectivity [109]. The generation rate and selectivity of H_2O-assisted CO_2 photocatalytic conversion and products (CO, H_2, and CH_4) over the Si, SiC, Pt/TiO_2, and GaN catalysts can be highly improved at high operating temperatures, as shown in Fig. 4d [96]. For instance, high photothermal behavior in Pt/TiO_2 [110] was obtained due to the light-driven thermocatalysis on Pt/TiO_2. Furthermore, the modification of TiO_2 with the MnO_x cluster induced a lower bandgap with abundant catalyst sites, resulting in higher photoactivity under visible light followed by efficient CO_2 reduction under low activation energies [80, 111].

The temperature interacts by thermally cleaving some molecules (C-O bond) whose photochemical surface reactions are kinetically limited or difficult to proceed for the creation of intermediates such as C and CO. It should be noted that the intermediates are further photochemically hydrogenated into CH_4/CO through the effects of e^-/h^+ recombination. The improvement in the photothermal CO_2 reduction rate is associated with the catalyst surface activity in terms of hot-electron photogeneration for the activation/absorption of intermediate reactions, the creation

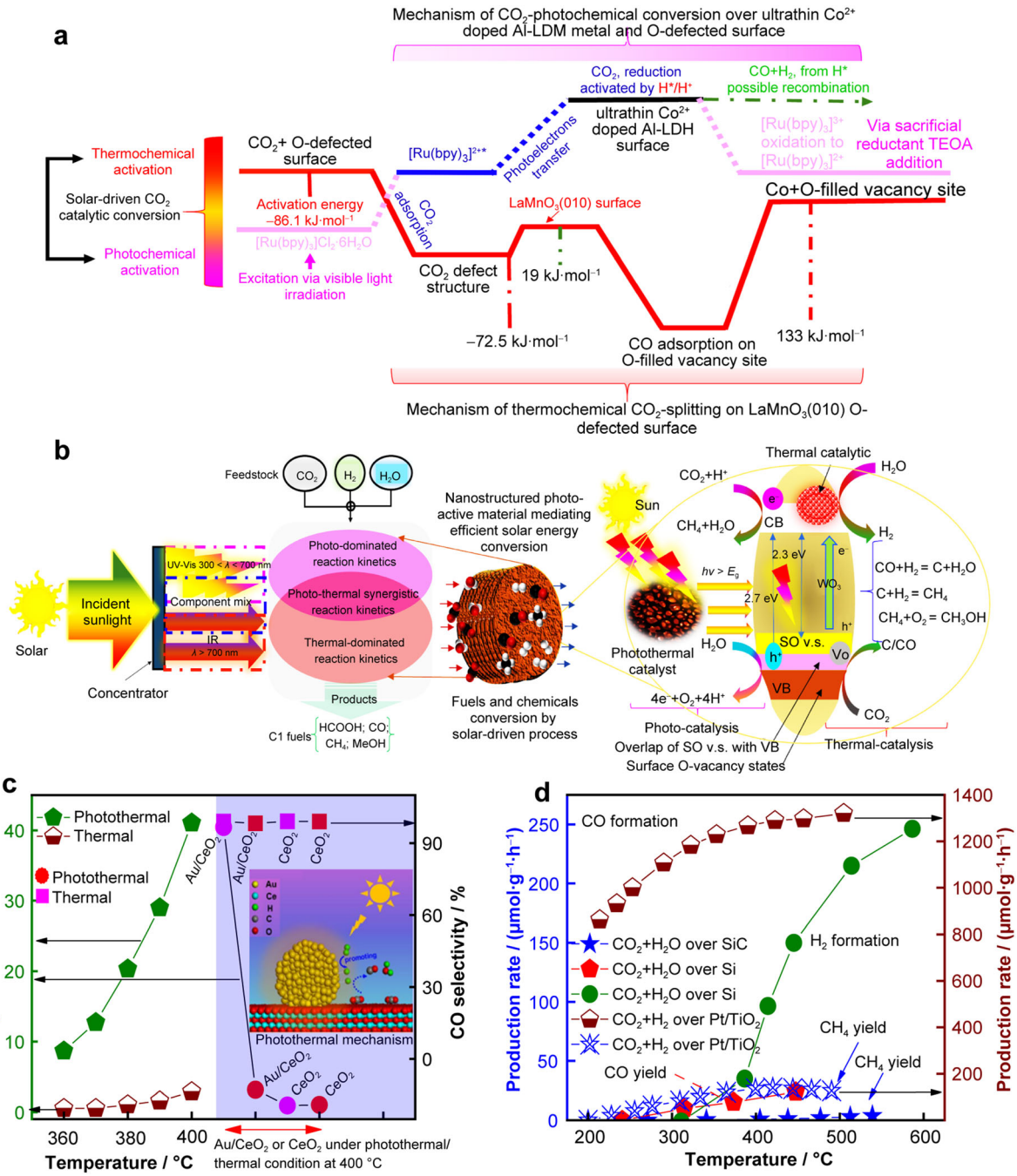

Fig. 4 Photothermal CO_2 catalytic conversion into fuel: **a** solar-driven CO_2 catalytic conversion mechanism. Reproduced with permission from Refs. [17, 101]. Copyright 2020, American Chemical Society. **b** Straightforward and effective method for whole range of solar spectrum utilization (nanostructured material mediating efficient conversion of solar energy, light, and heat joining force-driven solar energy conversion and heterogeneous photothermocatalysis mechanism). Reproduced with permission from Ref. [109]. Copyright 2016, the Royal Society of Chemistry. **c** CO_2 photothermal hydrogenation over an Au/CeO_2 heterostructure. Reproduced with permission from Ref. [2]. Copyright 2019, Elsevier. **d** Effect of temperature and photocatalyst activity toward major product (H_2, CO and CH_4) formation. Reproduced with permission from Ref. [96]. Copyright 2018, American Chemical Society

Table 2 CO_2 photothermal catalytic conversion under a broadband solar spectrum: Most relevant catalyst materials exhibiting photothermal properties and their catalytic activity toward CO_2 conversion under combined conditions are highlighted to provide insight into the available materials, their chemical compositions, and operating conditions compared to those used in a single photo- and thermochemical processes

Operating conditions	Fuels yield	Photocatalyst materials	Refs.
153 kW·m^{-2} of Av. radiation flux, T = 1000 °C, P = 0.101325 MPa, 1 L·min^{-1} of CO_2, 25 ml·min^{-1} of water vapor	8000 μmol·h^{-1} of CO	1 wt% Cu/TiO_2	[86]
300-W Xe lamp, 20 kW·m^{-2}; P = 0.20265 MPa; T = 150–190 °C; CO_2:H_2 = 1:1	22.0 μmol·g_{cat}^{-1}·h^{-1} of CO	$In_2O_{3-x}(OH)_y$/SiNW	[12]
300-W Xe lamp at 25 kW·m^{-2}; no filter; P = 0.186165 MPa; T = 160 °C; CO_2:H_2 = 1:1	11.7 mmol·g_{cat}^{-1}·h^{-1} of CO	$Pd@Nb_2O_5$	[106]
1000-W Xe lamp, $\lambda > 240$ nm; T = 250–350 °C	250 μmol·g^{-1}·h^{-1} of CO	Si	[96]
	35.8 μmol·g^{-1}·h^{-1} of CO, 35.4 μmol·g^{-1}·h^{-1} of CH_4	SiC	
	~ 3200 μmol·g^{-1}·h^{-1} of H_2	RuO_2/GaN:ZnO and $Rh_{2-y}Cr_yO_3$/GaN:ZnO	
Blue light with 450–460 nm at 300 °C, CO_2:H_2:N_2 = 1:4:1	94% CH_4 selectivity	Co_{10}/CeO_2	[87]
Green light of 560–570 nm at 450 °C, CO_2:H_2:N_2 = 1:4:1	100% CO selectivity	Cu_{10}/CeO_2	
300 UV–Vis spectrometer, P = 0.7579 MPa, T = 400 °C, PP_{CO_2} = 0.252863 MPa, PP_{H_2} = 0.505037 MPa, 15 cm^3·min^{-1} of total flow rate	2663 μmol·mg_{cat}^{-1}·min^{-1} of CO_2 conversion rate	Au/TiO_2	[99]
UV light of 365 ± 38 nm, 140 °C, atmospheric pressure, 30 (STP) L·h^{-1} He with 1 vol% CO_2, H_2O/CO_2 = 4	64 μmol·g^{-1}·h^{-1} of CH_4	Pd/TiO_2	[97]
Sunlight irradiation 14.5 kW·m^{-2}, at 300 °C	69.49 mmol·g_{cat}^{-1}·h^{-1} CH_4	1 wt% Ru/TiO_2	[89]
300-W xenon lamp (PLS-SXE300C), 138 °C, 2 ml H_2O, 1 ml CO_2	25.97 μmol·g^{-1}·h^{-1} of CO	2%CuS/TiO_2	[115]
300-W Xe lamp light $\lambda > 420$ nm, 250 °C	25.77 μmol·g^{-1} of CH_4	m-WO_3-H_{550}	[109]
1 sun illumination at 150 °C	85 mmol·g_{cat}^{-1}·h^{-1} CH_4	RuO_2	[122]
	135 mmol·g_{cat}^{-1}·h^{-1} CH_4	H_2 reduced RuO_2 into Ru under 2 h 250 °C	
300-W Xe lamp, at 365 °C	18.16 mmol·g_{cat}^{-1}·h^{-1} CH_4	Ru/Al_2O_3	[123]
300-W Xe lamp, at 285 °C	17 mmol·g_{cat}^{-1}·h^{-1} CH_4	Ni on $Ce_xTi_yO_2$ supports	[124]
UV light-emitting diodes, 30 W, λ = 380 nm; at 350 °C; H_2:CO_2 = 1	58.07 mmol·g_{cat}^{-1}·h^{-1}	$In_2O_{3-x}(OH)_y$	[125]
150 mW·cm^{-2}; T = 210 °C	12.4 mmol·g_{cat}^{-1}·h^{-1} of CH_4	Ru/TiNT	[126]
300-W Xe lamp irradiation, λ = 200–2000 nm; T = 400 °C; P = 0.18 MPa; 15 ml·min^{-1} flow rate; CO_2:H_2:Ar = 15:60:25	19.61 mmol·h^{-1}·g_{cat}^{-1} of CO over FeCe-300 (Fe:Ce = 2:1)	FeO-CeO_2	[127]

of O-vacancy in the support, and the effects of localized surface plasmon resonance (LSPR) of certain nanoparticles (Ni-, Rh-, Fe-, Au-, Ag-, Cu-, …) under light illumination [87, 99, 109, 112, 113]. In response to the challenges related to SPR-assisted C-O cleavage, coupling charge transfer and orbital in CO_2 photoreduction reaction mechanisms have been further investigated, resulting in a detailed mechanism of CO_2 to CO conversion over Au photocatalyst [114]. The combined properties were investigated by Ullah et al. [87] using $Co_{2.5}Cu_{7.5}/CeO_2$ as a bimetallic CO_2 photothermal reduction catalyst, reporting significant enhancements in the CO_2 conversion rate over the entire reaction temperature.

3.1.2 *Plasmon resonance excitation enhancing photothermal synergistic activity*

The use of a thermal mechanism in photocatalysis has been found to increase the CO_2 conversion rate over Ru/TiO_2 [89], CuS/TiO_2 [115], and Pd/TiO_2 [97], even at 150 °C. Compared to the single thermal process, this indicates that both spectral and intensity features are relevant. In that, the thermally driven mechanism in which increasing product formation with reaction temperature has been reported, the overall photothermal conversion efficiency relies on both photo- and thermal-driven reaction kinetics. In the photocatalytic reaction, it was found that doping the sample with

noble metals could result in the modification of the surface properties of the catalyst, thereby improving photoinduced electron–hole separation via the Schottky barrier, increasing the active sites formation, narrowing bandgap, and enhancing the catalyst activity due to the effects of SPR excitation under visible light and near IR [89, 97, 115, 116]. The Schottky barrier is a key factor for improving the photocatalyst activity of the semiconductor by appropriately doping or creating O-vacancies in the reacting interface [117]. From the thermodynamic perspective [89, 109], increasing the reaction temperature is the main enhancing factor for overcoming the photo-thermo insufficient driving forces (kinetics) for effective CO_2 conversion over 1–106 $W{\cdot}cm^{-2}$ light intensity [118].

A recent report indicated that a photothermal conversion of CO_2 into 7.5 $L{\cdot}m^{-2}{\cdot}h^{-1}$ CH_4 over two-dimensional amorphous Y_2O_3 nanosheets decorated with single Ni atoms (SA Ni/Y_2O_3) is possible with 0.52–0.7 $kW{\cdot}m^{-2}$ sunlight and at 288 °C with the use of a selective light absorption concept [119]. At high temperatures, light contributes to the reaction kinetics and product formation by reducing the activation energy of thermocatalytic reactions (for example, EaRu decreases from 70.4 to 36.2 $kJ{\cdot}mol^{-1}$) [118] via photoexcitation. The declination in the photogenerated charge carrier recombination dynamics resulting in the limitation in photo-oxidation kinetics at reaction temperatures exceeding the Debye temperature of the photocatalyst may be associated with nonradiative multi-phonon recombination of charge carriers [120]. The strongest catalysts for light-absorption behavior, such as Ru@FL-LDHs [42], are particularly effective for CO_2 reduction due to the strong binding capacity of Ru (2.4 eV) nanoparticles ($\geq$5 nm), followed by the bandgap energy reduction of the absorbed CO_2 (2.4–8.5 eV) [118]. The combination of these properties in the reacting media could result in boosting the overall photothermal catalytic activity [110]. The mixed metal oxidation state forming bifunctional catalysts, such as CuO/Cu_2O [121], can constitute part of an engineered photothermal catalyst design approach that could be crucial in photo- and thermocatalytic CO_2 reduction. This approach is attractive because of its reliability and operating temperature, below 600 °C [120], which is well suited to large-scale uses, such as demonstrations and industrial processing. Advanced catalysts of CO_2 photothermal catalytic conversion are highlighted in Table 2 [12, 86, 87, 89, 96, 97, 99, 106, 109, 115, 122–127] to provide comprehensive insights into the available materials developed to date, their chemical composition, photocatalytic performance, and appropriate operating conditions that could lead and ease future research direction toward higher performance and industrial scalability.

3.2 Design principles for a light-induced hot-electron thermal multi-field coupling heterogeneous reacting system

The possibility of a photothermal coupled process has been demonstrated for efficient CO_2 re-utilization into marketable energized products. However, light-thermal coupling principles, the optimal design of the photothermal bed, and the mechanisms underlying light-induced electron-thermal chemical energy storage are the major key scientific and engineering challenges (Fig. 5a). To address these issues, a photoinduced isomerization approach could be developed with thermochemical cycles for the direct storage of high energy spectral in heterogeneous catalysts and the direct utilization of unabsorbed photons for the synthesis of thermochemical fuels. This novel approach can generate a global solar-to-chemical energy conversion efficiency of 68.7% through numerical analysis [100]. Also, computational models accounting for fluid flow, heat and mass transfer, and radiation flux transport can be developed to study spectral coupled-intensity distribution characteristics and CO_2 photothermal conversion in a high light-transmission catalytic monolith porous medium. For instance, Bhatta et al. [94] reported a CO_2-to-CO conversion that was four times higher than the single thermochemical process at temperatures > 1000 °C due to the effect of photoenhanced thermal reaction in the reacting media [86, 128].

As shown in Fig. 5a, understanding the photothermal principles, mechanisms, and kinetics underpinning the theory of energy conversion from solar to fuels and chemicals could result in appreciable solar energy-conversion efficiencies. For instance, a higher H_2 production rate of up to 786 $\mu mol{\cdot}g^{-1}{\cdot}h^{-1}$ can be obtained with SiO_2/Ag@TiO_2 core–shell solar thermal collectors designed for photothermic-promoted hydrogen synthesis [129]. In addition, Pt/TiO_2-anchored photothermal bed could exhibit 4.2 and 8.1 times H_2 yield at 90 °C, relative to the single thermal- and photopowered reactor [130], respectively. Additionally, a windowed photoreactor covering a hot mirror is designed to split the solar beam into spectral and intensity [88]. This approach provides insight into developing a decoupled solar photothermal system based on an absorption-transmission fundamental mechanism. In a light-induced hot-electron and thermal coupling system, UV–Vis light-induced photons are directly exploited for photochemical performance, while the reflected incident radiation is concentrated on the active material for thermochemical conversion [131–133]. Taking a similar approach, Wang et al. [109], using the mechanism of CO_2 photothermocatalytic reduction over m-WO_{3-x}, have proposed the use of a photothermal reactor model that directly concentrates UV–Vis light at 780 nm > λ > 420 nm. However, to significantly improve CO_2 conversion and

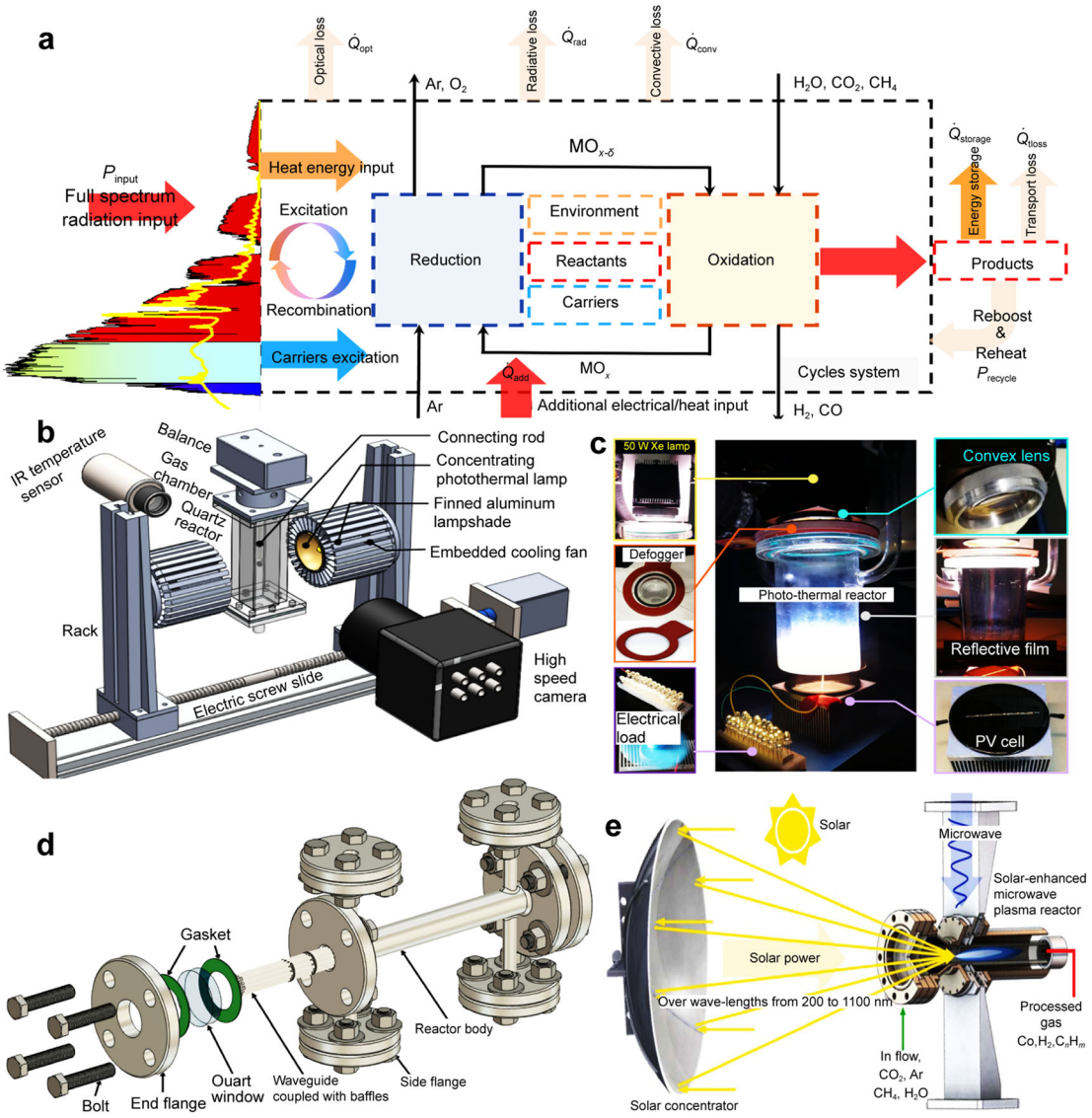

Fig. 5 Light-induced electron-thermal coupling energy storage system: **a** full-spectrum solar energy conversion process with detailed mass and energy flow diagram of overall process, optical loss, products and others; **b** high-concentration CO and CH_4 formation with a photothermal combustion reactor. Reproduced with permission from Ref. [141]. Copyright 2020, Elsevier. **c** Sunlight-to-photothermal H_2 generation and electricity by a PV cell. Reproduced with permission from Ref. [137]. Copyright 2020, iScience. **d** High-intensity light photothermal reactor for CO_2 conversion into fuels. Reproduced with permission from Ref. [125]. Copyright 2020, iScience. **e** Ultrahigh-temperature sunlight energy coupled microwave plasma reactor design for CO_2 re-use into fuels. Reproduced with permission from Ref. [142]. Copyright 2019, IOP Publishing Ltd

major product yields, such as CH_4 and CH_3OH, under the thermal and light-induced synergistic effects, the reactor is coupled with an additional solar-powered heating process.

A review of the literature related to the single thermal component of sunlight energy exploitation indicates that significant progress has been made in the design of solar thermal receivers and reactors for the performance of the synthesis of thermochemical fuels. However, recent scientific reports have been limited to a stable photothermal hybrid system design for fuel and chemical production due to the restricted understanding of the coupled-system conversion mechanisms, kinetics, and thermodynamic restrictions. Photocatalytic operating efficiency at elevated temperatures is a key issue associated with the combined system. Taking advantage of the issues related to photothermal heating along with light-induced charge-coupled

heat and mass transfer characteristics [134], as shown in Fig. 5d, a high-light intensity photothermal reactor has newly reported a photothermal catalytic CO_2 hydrogenation of up to 15.4 $mmol{\cdot}g^{-1}_{cat}{\cdot}h^{-1}$ of CO yield at 300 °C using $In_2O_{3-x}(OH)_y$ [125]. This catalyst system is considered the most appropriate photothermal catalyst at present [135]. Considering the recent literature and following the parent issues associated with a photothermal system, significant knowledge of thermochemical and photochemical systems and sufficient selectivity of the materials with significant photo and thermal properties could result in the effective configuration of a photothermal reactor.

The endothermic and exothermic nature of the RWGS reaction displaces the photon-thermal driven kinetic toward CO and MeOH synthesis at temperatures above 300 °C. A photoreactor carrying CO photothermal catalytic oxidation into CO_2 over Fe_3Si/Co_3O_4 has been developed with a maximal operating temperature of 250 °C at 1 $kW{\cdot}m^{-2}$ solar irradiation [136]. An advanced system design allowing for easy and efficient sunlight harvesting could produce photothermal fuels, chemicals, and electricity with 4.2% overall efficiency at 12 suns [137]. The photothermal catalytic activities have been tested at low temperatures because of the nonradiative recombination limitations subjected to a high-temperature thermal process. This issue could be surmounted by high-temperature photocatalyst engineering design, owing to significant knowledge of tunable parameters, including phonon dispersion characteristics, bandgap energies, trap, and vacancy or impurity states. Apart from the receiver configuration, the main difficulty in this process is the compromise in the thermal catalysis of terminal oxidants and their applicability in photoredox systems [138–140].

As depicted in Fig. 5b [141] and c [137], a quartz reactor coupled with a highly concentrating photothermal lamp can be developed for the photothermal catalytic reduction of CO_2 into fuel. In addition, the extended design of the newly developed photothermal reactor based on the light-thermal coupling concept using microwave plasma-enhancing solar fuels conversion is shown in Fig. 5e [142].

3.3 More distinct mechanisms underlying solar photothermal CO_2 catalytic reduction

It has been demonstrated that solar multi-spectral band radiative flux transfer, along with the generated heat transmission in a photoactive reacting media, could induce catalyst activation following reactive gas (CO_2) conversion through different reaction mechanisms, including photoinduced heating-mediated thermal catalysis, heat-mediated photocatalysis, and synergistic photothermal catalysis. Compared to the latter, where photocatalysis and thermocatalysis occur simultaneously, CO_2 conversion through thermal-assisted photocatalytic is typically based on the photocatalysis mechanism, while the light-assisted thermal CO_2 conversion process relies on the thermochemical mechanism. The limited knowledge of these distinct mechanisms restricts the efficient exploration of solar energy. Additionally, improving light-to-heat conversion efficiency, thermal management to enable efficient photothermal catalytic activity, and enhancing intrinsic catalytic site reactivity are critical factors that limit solar-to-chemical energy conversion efficiency. Research and innovative ideas are still needed to enhance optical and quantum efficiencies, spectral transfer, and heat transmission efficiency, as well as kinetic and thermodynamic of multiple electron transfer processes, and to find solutions for preventing electron–hole recombination and accelerating light-thermal energy conversion. This effort requires considerable focus on designing flow reactors and developing materials with better overall performance.

(1) Photoinduced heating-mediated thermal catalysis is mainly based on the thermal catalysis mechanism. The active catalyst material is heated to a desired temperature, leading to a chemical reaction upon light irradiation due to the spectral absorption capacity and plasmonic heating effects of the media. Under light irradiation, the catalyst adsorption energies (E_{ads}) capacity, with more negative E_{ads} indicating stronger adsorption, and reaction energies (ΔE) with negative ΔE representing exothermic process can be accessed through computational methods such as employing Vienna Ab-initio Simulation Package (VASP) combined with frozen-core projector augmented wave (PAW) methods [143]. The most significant issues are associated with the composition of the nanoparticle catalyst system, such as a cooperative catalyst system involving photocatalysts and photothermal catalysts and the catalyst synthesis conditions, particularly the preparation temperature and time. Considering 0.35Ru@O-vacancy-rich $Ni_2V_2O_7$ [144] and Ru/Mo_2TiC_2 [145] catalyst systems, the temperature of the reacting media rapidly increased under light illumination due to the high thermal conductivity of metal Ru, which acts as a light absorber and conversion into heat [146] following its high intrinsic activities exploited for the catalytic reactions. Regarding the structure and composition of the catalyst system, MXene-support seems to enable higher metal loading, enhance light absorption ability, and ensure thermal stability and long-term durability due to the stronger binding of the metal loaded and the support [147]. Besides, IR cameras and thermocouples carefully coupled to a flow reactor or batch reactor are usually employed to measure the surface

temperature change of the catalyst system. For light-assisted thermal reaction conducted in a flow reactor, the higher temperature of the reacting media first promotes energetic charge carriers transfer to the active sites and then induces fast desorption of H_2O followed by regeneration of the active catalyst sites, which lowers CO_2 activation energy barrier and creates more successful collisions. The protons created through photoactivity first weaken the C-O bond of the adsorbed CO_2 on the surface of the thermally activated oxygen carriers before it thermocatalytically converts into fuel driven by oxygen vacancies [148]. Afterward, the lattice oxygen is extracted from the oxide surface, followed by the formation of H_2O and regeneration of oxygen vacancies due to the activity of protons. The process of photoinduced charge carrier transfer that can be permanent or transient is attributed to photochemical activation, allowing high-temperature reactions to occur under milder conditions. The localized heat generation [144, 149] responsible for the thermocatalytic-driven reaction could be more favored by doping high thermal conductivity semiconductors with poor thermal conductivity photocatalysts used as the major light absorber. It should be noted that the local thermal effect is mainly attributed to the fast recombination of the photogenerated e^-/h^+ pairs, and the rapid increase in the local temperature can be observed due to the IR shielding effect, heat transfer between catalyst and substrate, and heat preservation when the support matrix is made of high thermal conductivity metal oxides [150, 151]. The material possessing strong light-absorbing capacity, hot-electron generation, higher heating effect, and unique catalytic function could be preferable for achieving high-efficiency CO_2 thermocatalytic conversion due to the strong implication of photoenhanced reactivity and selectivity [68, 152, 153]. In addition, most of the literature reported a higher catalytic rate under Xe lamp irradiation rather than in the dark under thermal heating conditions, which justifies the higher contribution of photogenerated energetic charge carriers in the traditional thermocatalytic reaction [154].

(2) In the heat-mediated photocatalysis process, mainly driven by the photocatalysis mechanism, a high CO_2 conversion rate is strongly associated with stronger CO_2 adsorption achieved via increasing temperature that can be controlled through heating. Also, boosted photocatalytic CO_2 reduction performance can be obtained by enhancing CO_2 adsorption capacity while increasing the surface-active sites and improving charge separation/transfer through the composite catalyst system [155–157]. A stronger CO_2 adsorption capacity over two-dimensional catalysts such as Co-$Ti_3C_2T_x$ was observed by increasing the temperature, which indicated a strong implication of temperature in the photocatalytic CO_2 conversion process [158, 159]. However, the photodriven reaction mechanism may upgrade to the conventional thermocatalytic process, thereby resulting in less photocatalytic activity due to the photocatalyst sintering and deactivation in long-term high-temperature environments.

(3) Synergistic photothermal catalysis typically combines photocatalysis and thermocatalysis mechanisms, where the reaction kinetics and high product selectivity are promoted by photothermal heating and photoexcited charge transfer processes simultaneously. Recently, experimental tests were conducted under dark at room temperature, dark at high temperature, 300-W Xe lamp irradiation leaching IR light, and full-Arc 300-W Xe lamp irradiation to disclose the contributions of light and heat in the solar-driven CO_2 conversion over catalytic reaction. Through the above experimental proceeding, Chen et al. [144] reported a high amount of CH_4 production of 9.2 times higher than the thermal catalytic activity and 3.9 times higher than the sum of photocatalytic and thermal catalytic activities, demonstrating the high involvement of the photo- and photothermal catalytic synergetic effects. Besides, the incident light wavelength and the absorption edge of the catalyst could be regarded as the controlling factors to regulate CO_2 reduction photocatalytic and thermocatalytic activities mainly driven by photogenerated e^-/h^+ pairs and local thermal effect, respectively. For instance, the photons absorbed in the catalyst system could photothermally activate chemical reactions through the thermal effect for the wavelength greater than the catalyst absorption edge. Besides adopting the MXene structure as photothermal support, Wu et al. [160] obtained exceptional light absorption capacity, resulting in higher surface temperature due to the intrinsic thermocatalytic activity of Ni/Ti_3C_2. MXene-based material can be considered a promising photothermal catalyst due to its excellent photothermal characteristics, such as strong light absorption and heat management capacity, as well as multi-functional surface reactivity [161]. The CO_2 hydrogenation reaction through photothermal catalysis proceeds via H_2 activation followed by metal-H formation, which is the determining factor for subsequent CO_2 or the activated form of CO_3^{2-} conversion across the interface between metal nanoparticles and the support matrix [106, 162]. This indicated that gas phase reactant adsorption on the catalyst surface could be regarded as the first step of the photothermal catalytic reaction, which could be promoted by

increasing the basic site on the catalyst surface. Ren et al. [42] reported that targeting and activation of CO_2 and H_2 simultaneously on the support matrix and nanoparticle catalyst surface could result in high-efficient CO_2 photothermal reduction. Interestingly, the conversion rate and high selectivity strongly depend on the interaction between the metal catalyst and the support matrix, implying the necessity of deep research on how the electronic properties of a metallic catalyst are modified by the support to shift the selectivity to desired products [163–165]. Accordingly, recent studies increasingly consider theoretical studies such as employing density functional theory (DFT) calculations and in-situ characterization methods to unveil the electronic properties of catalyst systems, as well as in-depth analyses of catalytic reaction pathways and the reaction intermediates. Still, the photothermal property and the intrinsic thermal catalytic reactivity of the catalyst are crucial for accessing high-efficiency photothermal performance. This makes the photothermal reaction look similar to the conventional thermocatalysis apart from the presence of light, which alters the reaction mechanism to the photothermal, thereby excluding the photocatalysis reaction coordinate. Besides, broadening solar absorption and improving heat transfer efficiency along with the active sites via incorporating dopants have been suggested as the key challenging issues for achieving higher CO_2 photothermocatalytic conversion performance and selectivity [166–168].

The catalytic reacting media in which photocatalysis and thermocatalysis occur under solar irradiative flux could be regarded as a complex coupling process. However, the mechanisms underlying sunlight-efficient harvesting and CO_2 reduction employing composite catalyst are only understood from the basic mechanism, including photo- and thermocatalytic activity induced by the catalyst system under light irradiation [149, 169]. In contrast, the effects of other decisive phenomena induced simultaneously by light and thermal are still unclear. To this end, intensive efforts not only on the material but also more focused on the physical model-integrated photothermal catalysts should be devoted to providing a reliable photothermocatalysis system for an effective demonstration as experienced with the high-temperature thermochemical processes.

4 Conclusions, limitations, and perspectives

The reliability and effectiveness of using solar irradiation to convert CO_2 into sustainable value-added fuel and chemical energy have been proven, and it could be expected to become a low-cost renewable and net-zero carbon emission technology for synthesizing industrial raw materials. The main research fields and focus mainly involve (i) optimization and dynamic regulation of the optical systems for enhancing the optical and absorption efficiency up to the maximum usage of the incident irradiation; (ii) the design, preparation, and intensive studies on material and reactor structures along with reaction processes to achieve fully the usage of external energy applied; and (iii) intensive studies on the performance evolution and regulation of the photothermal effect to upgrade solar energy conversion efficiency. Although exponentially growing research trends have been observed, this emerging technology cannot fully realize its engineering application potential due to the lack of mature photothermal catalysts, lack of photothermocatalytic reactors development, and limited understanding of the underlying techniques and methods. A summary analysis of the mechanisms underlying the photocatalytic and thermocatalytic CO_2 conversion showed a daunting challenge associated with improving the solar photothermocatalytic conversion efficiency regarding large-scale demonstration and applications.

4.1 Key performance

Remarkable yields of clean combustible fuels ([H_2/ + CO], CH_4, MeOH and C2+) were reported, indicating the techno-economic feasibility and technological readiness for possible industrialization, as well as for green environmental remediation. UV–visible light, efficient distribution and absorptivity, CO_2 binding and activation capacity, active catalyst porosity, and charge transfer are the inherent characteristics of the photochemical reaction chamber for efficient CO_2 conversion. H_2 formation and selectivity were favored by photoactivity relative to CO yield. It seems that light-induced hot-electrons are less favored for splitting CO_2, considering the amount of H_2 produced and the CO generation rate of about 91.9 and 4.97 $mmol{\cdot}g^{-1}{}_{cat}{\cdot}h^{-1}$, respectively, through pg-C_3N_4/Ti_3AlC_2/TiO_2. As shown in Fig. 6b, important results regarding Pt/In_2O_3/g-C_3N_4, u-CoAl-LDH, pg-C_3N_4/Ti_3AlC_2/TiO_2, Au_{20}@ZIF-67, $Ni_{0.75}Mg_{0.25}$-MOF-74 and $Bi_{12}O_{17}Br_2$ nanotubes indicate significant CO yield, as well as other major fuels (HCOOH, MeOH, ethanol and H_2), from 566.4 $\mu mol{\cdot}g^{-1}$ up to $\sim$ 736.3 $mmol{\cdot}g^{-1}{\cdot}h^{-1}$ under visible light irradiation. While using the materials' O_2 extraction/uptake behavior, CeO_2/$CeO_{2-\delta}$, $Fe_{0.35}Ni_{0.65}O_x$, $LaCo_{0.7}Zr_{0.3}O_3$, $Ce_{0.75}Zr_{0.25}O_2$-C, $Pr_{0.18}Sr_{0.80}Mn_{0.99}O_{2.951}$, and $Pr_{0.39}Sr_{0.63}Mn_{0.98}O_{2.979}$ resulted in much more

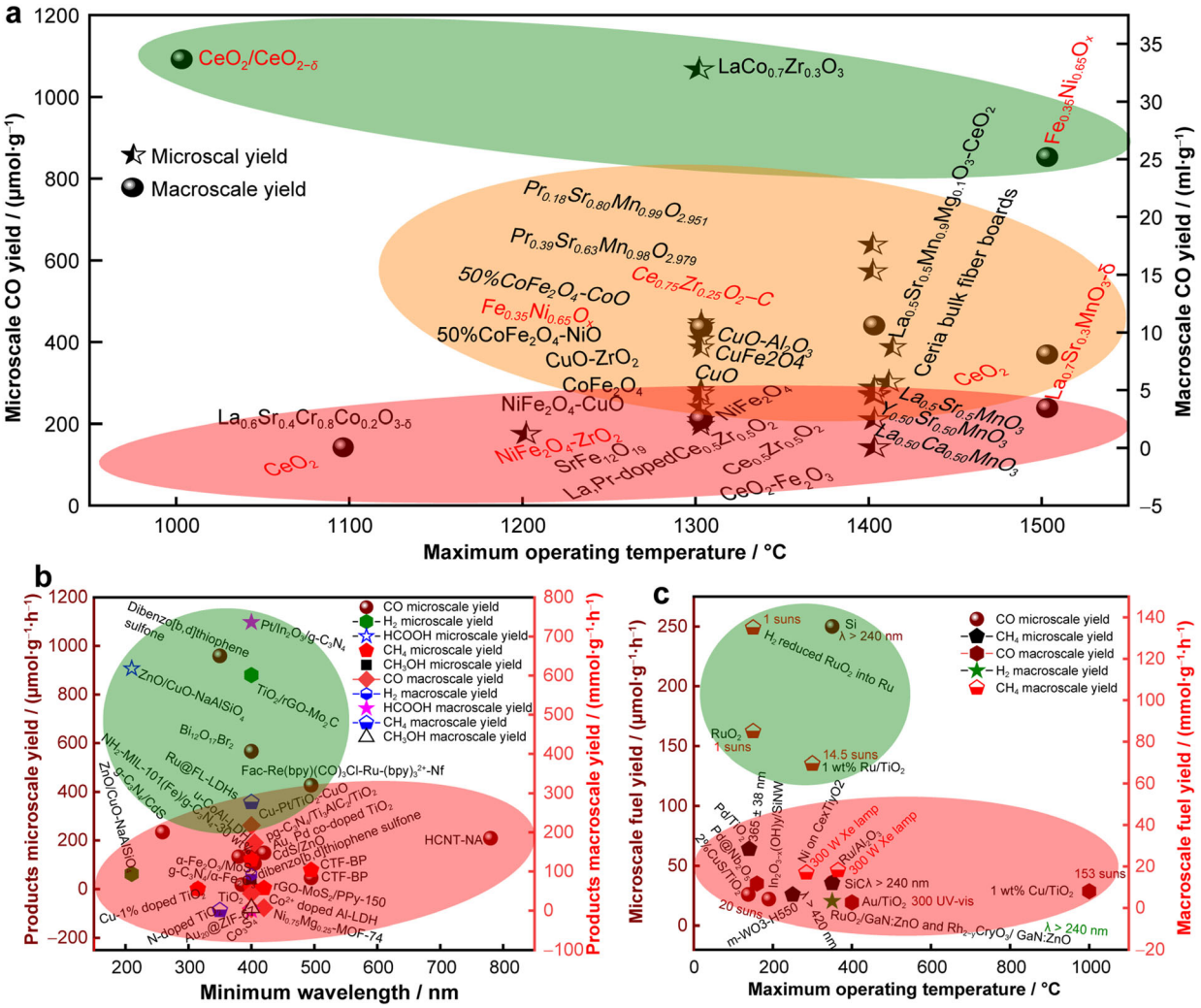

Fig. 6 CO_2 photothermal catalytic conversion potential at micro–macroscale highlighted from the most promising catalysts available in database: **a** potential thermal catalysts and CO-conversion efficacy; **b** most investigated photocatalysts and CO-generation rate as a function of wavelength; **c** catalysts presenting both thermal and photo properties and CO productivity over reaction temperature and light intensity changes (data from Table 1 and Table 2)

favorable redox thermodynamic characteristics regarding CO_2 conversion, to about 500–1500 μmol·g^{-1} of CO yield, as shown in Fig. 6a.

Considering the photocatalyst mechanism and thermodynamic limitations, active atomic surface tensile strain is highly relevant to the hot-electron transfer and effective charge separation toward high product selectivity. However, understanding the electronic structure and atomic coordination of the dynamic evolution of CO_2 subjected to photoreduction remains limited. Although photocatalyst activity favors H_2 generation, the current materials are limited by their low quantum efficiency and chemical or physical instability [170]. Most studies have been conducted on the photocatalyst level, resulting in a trade-off in the final yield of photogenerated fuels that can be considered major scientific issues for understanding the inherent mechanisms and kinetics of in-situ CO_2 photoreductions through an appropriate optofluidic reactor model. The development of photocatalytic reactors has not seen the enormous progress achieved in thermochemical or thermal reactors.

4.2 Photothermal system and future research

When combined with thermal elements, the photocatalyst conversion rate becomes more significant for catalysts with higher in-situ heating effects. The nonradiative relaxation of active catalysts associated with the optical excitation of intra-/interband electrons and the plasmon resonance effect is relevant to CO_2 binding and photothermal reduction. The maximum operating temperature for overcoming the insufficient photothermal driving forces to efficiently

exploit the synergistic photothermal effects is about 600 °C. Increasing reaction temperatures beyond 600 °C could result in single thermal-driven reaction kinetics. Photo-/thermalenhanced CO_2 conversion kinetics is significant for both photochemical and thermochemical processes, namely, in improvements to the generation efficiency of solar fuels in the literature. Further fundamental research is needed to develop rigorous and comprehensive multi-physics models for light-induced hot-electron and thermal-coupled systems to obtain an understanding of the in-situ mechanisms, kinetics, and thermodynamics that could lead to the appropriate design of a photothermal system. Surface chemistry is the most pronounced kinetic for both photo- and thermocatalytic chemical conversions. However, lowering the activation energy for the thermal catalyst and narrowing the bandgap of the photocatalyst are two major considerations that could illuminate the black box, constraining the development trends in the photothermal discipline.

Appropriate photothermal catalysts exhibiting significant CO_2 thermal and photocatalytic conversion are presented in Fig. 6c to highlight the catalyst materials

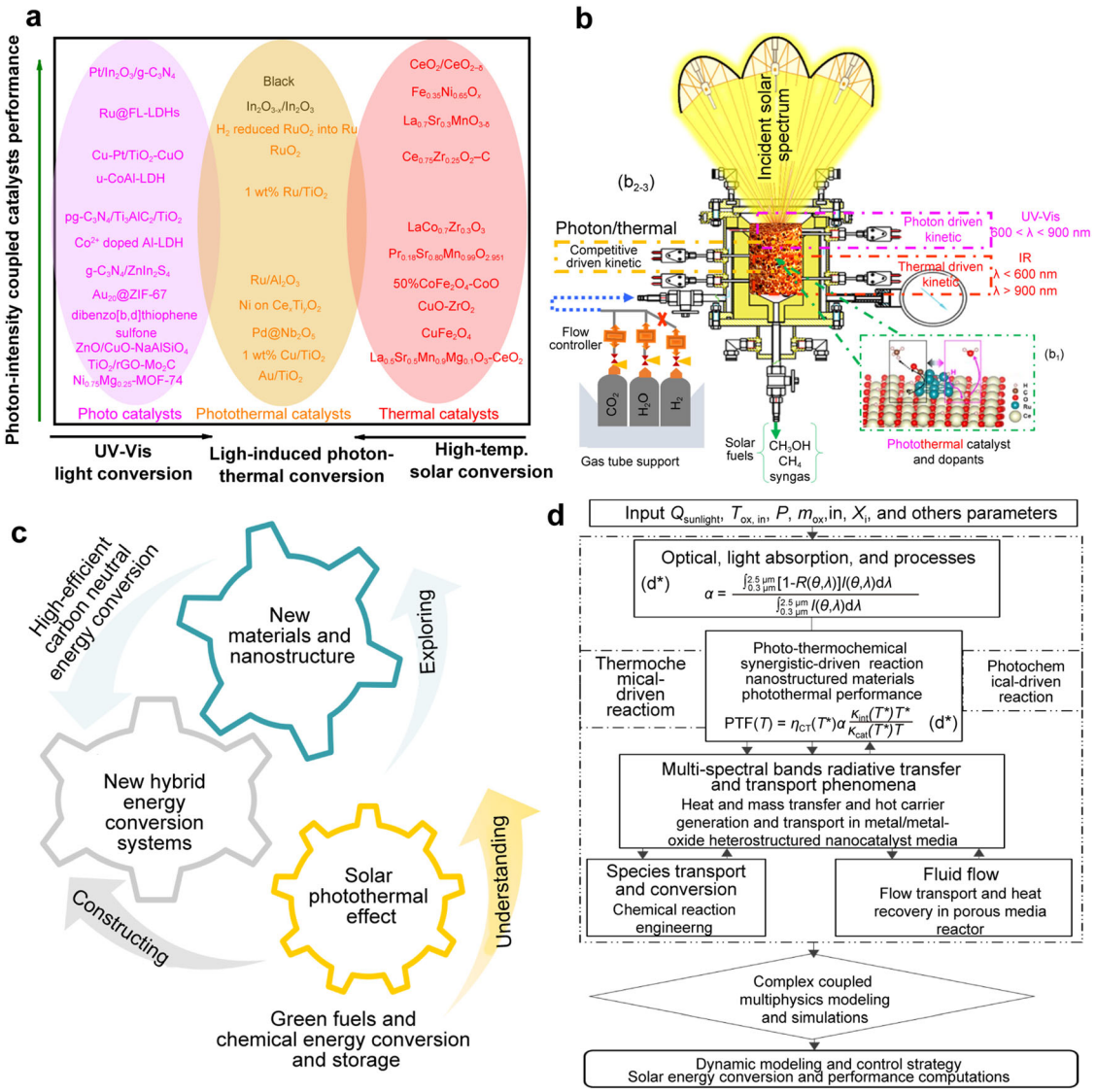

Fig. 7 **a** Material by design approach easing photocatalytic upgradation to low-temperature solar fuels and chemical energy storage; **b** coupled spectral and intensity enhancing CO_2 re-use for full-spectrum solar energy utilization into marketable energizing products in an optofluidic photothermal reactor. **b1** Reproduced with permission from Ref. [171]. Copyright 2018, American Chemical Society; **b2** reproduced with permission from Ref. [3]. Copyright 2018, Elsevier and Science Press; **b3** reproduced with permission from Ref. [131] Copyright 2023, Elsevier. **c** Way to future development; d solar photothermal system dynamic behavior modeling and control strategy. **d*** Reproduced with permission from Ref. [149]. Copyright 2019, Elsevier

development dynamic. A similarity is observed in the materials selection and chemical composition, indicating that the same single-atom catalyst or composite catalyst can perform well under UV–Vis light or thermal conditions. During catalyst selection, the photoexcitation of the active catalyst results in the reduction of the material's activation energy during the thermochemical process, whereas, in the case of photochemical processes, the thermal effect induces the bandgap energy reduction of the active material. UV–Vis light and high-temperature driven chemical reaction upgradation to reasonable and highly efficient photon/thermal system was only possible by taking advantage of the underlying catalyst-based sunlight energy conversion and reactive flow properties as shown in Fig. 7a. Among the catalysts reported to date, Ru catalysts, particularly H_2, which reduces RuO_2 into active Ru catalyst and black In_2O_{3-x}/In_2O_3 redox catalyst, have emerged as parts of advanced catalytic systems exhibiting remarkable photothermal catalyst activity for efficient CO_2 conversion and high product selectivity. These photothermal concepts and principles go beyond a simple summary of photo and thermal effects due to competitive or synergistic photothermal chemical reaction kinetics and SPR effects of plasmonic materials, making the process more relevant in terms of global application.

4.3 Path toward a sustainable solar-driven approach to catalysis system design

New insights have been gained into the design of functional and active catalysts and their efficiency and stability in a flow reaction system, as seen in Fig. 7b [3, 131, 171], which has significantly advanced the research trend of converting solar energy into fuel and chemicals, exploiting both spectral and solar intensities. The recent literature in the field indicates that CO_2 catalytic hydrogenation, considered the key process for the current new chemical industry, appears to be an appropriate way to achieve full-spectrum solar energy conversion into fuels and chemicals. A remarkable fuel yield was obtained with the RWGS process, which was thus suitable to the photon and heat content of solar energy, harnessed into selective products. Taking advantage of the thermodynamic and kinetic restrictions subjected to a single solar spectrum component, introducing light into the thermochemical process and vice-versa is a great challenge to achieving high CO_2 re-use. An optofluidic bed-design approach for improving photothermal catalysis under reactant coupling light and heat-enhanced chemically reacting media has been demonstrated to provide an engineered design approach. Other specific cases that require intensive study, along with their associated difficulties, pose key challenges in the future, as shown in Fig. 7c.

There are significant signs of progress in developing a photothermal catalyst system that could make full-spectrum solar energy integration more widespread. Some existing fluidized bed solar reactor configurations that are energy intensive, highly costly, safe, and stable can be easily modified into light absorbers to create a photothermal process for the coupling photon-thermal performance. Energy savings of up to 63% were achieved by integrating UV–Vis light into a thermal reactor while maintaining a tremendous amount of chemical conversion [118]. A selective light absorption approach was found to be an appropriate concept for improving the temperature distribution within the photothermal catalyst system at ambient solar irradiation. In addition to other influencing factors, the residence time (reactor volume (V)/flow-rate (v)), in terms of short and long time corresponding to high flow and low flow rates, resulted in lower and higher CO_2 conversion, respectively. To deeply investigate the coupling effect of solar photo energy and thermal energy in which the photocatalysis and thermocatalysis take part synergistically in the catalytic reactions, it is imperative to design a scalable photothermocatalysis reactor that best utilizes the catalyst materials to maximize solar energy conversion and major product selectivity. Figure 7d [149] is a simplified physical model of light-thermal-chemical multi-field coupling dynamic behavior modeling and control strategy that can be developed using finite element method (FEM), computational fluid dynamic (CFD) codes, Monte-Carlo rays tracing method, and other relevant software considering real data of solar field (optical system). Ultimately, the established numerical models can be applied to search for the principles of coupling solar energy and thermal energy, study multi-spectral bands radiative transport and optical efficiency improvement, and design and optimize optofluidic reactor and porous structure.

This insight is closely tied to the fundamental insight of the photothermal approach, combining light and heat to provide an alternative approach for the industrial outflow of CO_2 re-use into major products such as CH_4 and MeOH with more effective CO_2 conversion rates than the most challenging single photocatalytic component. The success of such a technology could promote renewable, clean fuel and chemical production and systematically impact global economic trends and green environment remediation. The formation rates of CH_4 and MeOH may be affected by the yield of CO due to the effects of surface-frustrated Lewis pairs, which are found in the photocatalytic mechanism. As shown in Fig. 6, much work has reported CO, CH_4, MeOH, and HCOOH as major fuels produced from CO_2 photothermal conversion, owing to the limitations of photon-thermal kinetics. These are still attractive compared to the single-photo- or thermochemical processes. The O-vacancies activity of the surface of a metal oxide is the

determining factor for controlling the yield of MeOH and CH_4, thanks to the active sites-based CO_2 photothermo-catalytic conversion mechanism. The plasmonic heating contribution in the media remains a black box when light is introduced to the thermal process due to the self-generation behavior of the specific metal catalysts at a microscale connected to plasmonic hot-electron heating that may dominate the system's macroscale temperature changes. In certain cases, the thermal contribution may alternate with photon-driven kinetics at high light intensities of about 5.7 and 8.5 suns [122]. Thus, it compromises the effective photothermal-driven kinetics regarding the complexity of exploiting the synergistic mechanisms of hot-electrons and heating phenomena [172–174].

The black-colored catalyst seen in Fig. 7a may present Vis-light absorption above 600 nm by promoting UV–Vis light to heat conversion, and as a result, produce higher photothermal catalytic activity [175] as is observed from black In_2O_{3-x}/In_2O_3 exhibiting 100% CO selectivity compared to the yellow one [148]. Several typical photothermal materials, including semiconductors with a narrow bandgap (Ti_2O_3, Fe_3O_4 and black titania), metallic nanoparticles (plasmonic noble metal (Au, Ag and Ru) and non-precious metals (Al, Cu, Nb, Ni and Fe)), carbonaceous materials (biomass-derived amorphous carbon, graphene, GO, rGO and CNTs), MOFs, and MXenes ($M_{n+1}X_nT_x$ (n = 1–3), M = Sc, Ti, Zr, Hf, V, Nb, Ta, Cr, or Mo; X = carbon or nitrogen; T_x = oxygen, hydroxyl, and fluorine) have been illustrated to guide the design of photo-thermocatalysis system. Regarding the study developed by Tang et al. [137], it is evident that the photothermal processes have a long course to successfully realize fuel production from sunlight, mainly due to poor photo- and thermoresponsiveness to UV–Vis light and heat coordinates, resulting in larger recombination and heat losses of 22.10% and 24.16%, respectively. Ultimately, this study highlights and draws attention to the most significant breakthroughs to overcome the current key challenges and future research dynamics in CO_2 reuse through a photothermal catalysis system.

Acknowledgments This study was financially supported by the China National Key Research and Development Plan Project (No. 2018YFA0702300) and the National Natural Science Foundation of China (No. 52227813).

Declarations

Conflict of interests The authors declare that they have no conflict of interest.

References

[1] Zhai S, Rojas J, Ahlborg N, Lim K, Cheng CHM, Xie CL, Toney MF, Jung IH, Chueh WC, Majumdar A. High-capacity thermochemical CO_2 dissociation using iron-poor ferrites. Energy Environ Sci. 2020;13(2):592. https://doi.org/10.1039/c9ee02795e.

[2] Lu BW, Quan FJ, Sun Z, Jia FL, Zhang LZ. Photothermal reverse-water-gas-shift over Au/CeO_2 with high yield and selectivity in CO_2 conversion. Catal Commun. 2019;129:105724. https://doi.org/10.1016/j.catcom.2019.105724.

[3] Guene Lougou B, Shuai Y, Chaffa G, Xing H, Tan HP, Du HB. Analysis of CO_2 utilization into synthesis gas based on solar thermochemical CH_4-reforming. J Energy Chem. 2019;28:61. https://doi.org/10.1016/j.jechem.2018.01.011.

[4] Jiang BS, Sun QM, Guene Lougou B, Zhang H, Li X, Qu ZB, Shuai Y, Wang CH. Highly-selective CO_2 conversion through single oxide CuO enhanced $NiFe_2O_4$ thermal catalytic activity. Sustain Mater Technol. 2022;32:e00441. https://doi.org/10.1016/j.susmat.2022.e00441.

[5] McDaniel AH, Miller EC, Arifin D, Ambrosini A, Coker EN, O'Hayre R, Chueh WC, Tong JH. Sr- and Mn-doped $LaAlO_{3-\delta}$ for solar thermochemical H_2 and CO production. Energy Environ Sci. 2013;6(8):2424. https://doi.org/10.1039/c3ee41372a.

[6] Chueh WC, Falter C, Abbott M, Scipio D, Furler P, Haile SM, Steinfeld A. High-flux solar-driven thermochemical dissociation of CO_2 and H_2O using nonstoichiometric ceria. Science. 2010;330(6012):1797. https://doi.org/10.1126/science.1197834.

[7] Yuan H, Mei JH, Gong YN, Zhong DC, Lu TB. Cobalt-based heterogeneous catalysts for photocatalytic carbon dioxide reduction. Tungsten. 2023. https://doi.org/10.1007/s42864-023-00208-2

[8] Liu Y, Zhang ZY, Fang YR, Liu BK, Huang JD, Miao FJ, Bao YN, Dong B. IR-Driven strong plasmonic-coupling on Ag nanorices/$W_{18}O_{49}$ nanowires heterostructures for photo/thermal synergistic enhancement of H_2 evolution from ammonia borane. Appl Catal B. 2019;252:164. https://doi.org/10.1016/j.apcatb.2019.04.035.

[9] Abanades JC, Rubin ES, Mazzotti M, Herzog HJ. On the climate change mitigation potential of CO_2 conversion to fuels. Energy Environ Sci. 2017;10(12):2491. https://doi.org/10.1039/c7ee02819a.

[10] Wang W, Deng CY, Xie SJ, Li YF, Zhang WY, Sheng H, Chen CC, Zhao JC. Photocatalytic C-C coupling from carbon dioxide reduction on copper oxide with mixed-valence copper(I)/copper(II). J Am Chem Soc. 2021;143(7):2984. https://doi.org/10.1021/jacs.1c00206.

[11] Song CQ, Wang ZH, Yin Z, Xiao DQ, Ma D. Principles and applications of photothermal catalysis. Chem Catal. 2022;2(1):52. https://doi.org/10.1016/j.checat.2021.10.005.

[12] Hoch LB, O'Brien PG, Ali FM, Sandhel A, Perovic DD, Mims CA, Ozin GA. Nanostructured indium oxide coated silicon nanowire arrays: a hybrid photothermal/photochemical approach to solar fuels. ACS Nano. 2016;10(9):9017. https://doi.org/10.1021/acsnano.6b05416.

[13] Gao JX, Tian WJ, Zhang HY. Progress of Nb-containing catalysts for carbon dioxide reduction: a minireview. Tungsten. 2022;4(4):284. https://link.springer.com/article/10.1007/s42864-022-00185-y.

[14] Liu Q, Wu LP, Jackstell R, Beller M. Using carbon dioxide as a building block in organic synthesis. Nat Commun. 2015;6:5933. https://doi.org/10.1038/ncomms6933.

[15] Majumdar A, Deutch J. Research opportunities for CO_2 utilization and negative emissions at the gigatonne scale. Joule. 2018;2(5):805. https://doi.org/10.1016/j.joule.2018.04.018.

[16] Davis SJ, Lewis NS, Shaner M, Aggarwal S, Arent D, Azevedo IL, Benson SM, Bradley T, Brouwer J, Chiang YM, Clack CTM, Cohen A, Doig S, Edmonds J, Fennell P, Field CB,

Hannegan B, Hodge BM, Hoffert MI, Ingersoll E, Jaramillo P, Lackner KS, Mach KJ, Mastrandrea M, Ogden J, Peterson PF, Sanchez DL, Sperling D, Stagner J, Trancik JE, Yang CJ, Caldeira K. Net-zero emissions energy systems. Science. 2018; 360(6396):eaas9793. https://doi.org/10.1126/science.aas9793.

[17] Bai S, Wang ZL, Tan L, Waterhouse GIN, Zhao YF, Song YF. 600 nm irradiation-induced efficient photocatalytic CO_2 reduction by ultrathin layered double hydroxide nanosheets. Ind Eng Chem Res. 2020;59(13):5848. https://doi.org/10.1021/acs.iecr.0c00522.

[18] Chandrasekaran S, Bowen C, Zhang PX, Li ZL, Yuan QH, Ren XZ, Deng LB. Spinel photocatalysts for environmental remediation, hydrogen generation, CO_2 reduction and photoelectrochemical water splitting. J Mater Chem A. 2018;6(24): 11078. https://doi.org/10.1039/c8ta03669a.

[19] Cheng RX, Qi CR, Wang L, Xiong WF, Liu HJ, Jiang HF. Visible light-promoted synthesis of organic carbamates from carbon dioxide under catalyst- and additive-free conditions. Green Chem. 2020;22(15):4890. https://doi.org/10.1039/d0gc00910e.

[20] Li PX, Yan XY, Song XM, Li JJ, Ren BH, Gao SY, Cao R. Zirconium-based metal–organic framework particle films for visible-light-driven efficient photoreduction of CO_2. ACS Sustain Chem Eng. 2021;9(5):2319. https://doi.org/10.1021/acssuschemeng.0c08559.

[21] Li ZH, Shi R, Ma YN, Zhao JQ, Zhang TR. Photodriven CO_2 hydrogenation into diverse products: recent progress and perspective. J Phys Chem Lett. 2022;13(23):5291. https://doi.org/10.1021/acs.jpclett.2c01159.

[22] Bingham M, Mills A. Catalytic and photocatalytic water gas shift reaction (WGSR) using a continuous flow, gas phase reactor. J Photochem Photobiol, A. 2021;409:113133. https://doi.org/10.1016/j.jphotochem.2021.113133.

[23] Zhu ZJ, Tang R, Li CR, An XD, He L. Promises of plasmonic antenna-reactor systems in gas-phase CO_2 photocatalysis. Adv Sci. 2023;10(24):2302568. https://doi.org/10.1002/advs.202302568.

[24] Xi YY, Cai MJ, Wu ZY, Zhu ZJ, Shen JH, Zhang CC, Tang R, An XD, Li CR, He L. Identification of photochemical effects in Ni-based photothermal catalysts. Chin J Struct Chem. 2023; 42(6):100071. https://doi.org/10.1016/j.cjsc.2023.100071.

[25] Agbe H, Nyankson E, Raza N, Dodoo-Arhin D, Chauhan A, Osei G, Kumar V, Kim KH. Recent advances in photoinduced catalysis for water splitting and environmental applications. J Ind Eng Chem. 2019;72:31. https://doi.org/10.1016/j.jiec.2019.01.004.

[26] Yuan L, Xu YJ. Photocatalytic conversion of CO_2 into value-added and renewable fuels. Appl Surf Sci. 2015;342:154. https://doi.org/10.1016/j.apsusc.2015.03.050.

[27] Becerra J, Nguyen DT, Gopalakrishnan VN, Do TO. Plasmonic Au nanoparticles incorporated in zeolitic imidazolate framework (ZIF-67) for efficient sunlight-driven photoreduction of CO_2. ACS Appl Energy Mater. 2020;3(8):7659. https://doi.org/10.1021/acsaem.0c01083.

[28] Cai XT, Wang F, Wang RX, Xi YM, Wang A, Wang JW, Teng BT, Bai S. Synergism of surface strain and interfacial polarization on Pd@Au core–shell cocatalysts for highly efficient photocatalytic CO_2 reduction over TiO_2. J Mater Chem A. 2020;8(15):7350. https://doi.org/10.1039/d0ta01247e.

[29] Feng XY, Liu ZY, Qin LX, Kang SZ, Li XQ. Photocatalytic activity and the electron transport mechanism of titanium dioxide microsphere/porphyrin implanted with small size copper. Phys Chem Chem Phys. 2020;22(24):13528. https://doi.org/10.1039/d0cp01953d.

[30] Li JY, Yuan L, Li SH, Tang ZR, Xu YJ. One-dimensional copper-based heterostructures toward photo-driven reduction of CO_2 to sustainable fuels and feedstocks. J Mater Chem A. 2019;7(15):8676. https://doi.org/10.1039/c8ta12427b.

[31] Chen Y, Zhao YF, Yu B, Wu YY, Yu XX, Guo SE, Han BX, Liu ZM. Visible light-driven photoreduction of CO_2 to CH_4 over TiO_2 using a multiple-site ionic liquid as an absorbent and photosensitizer. ACS Sustain Chem Eng. 2020;8(24):9088. https://doi.org/10.1021/acssuschemeng.0c02333.

[32] Dao XY, Xie XF, Guo JH, Zhang XY, Kang YS, Sun WY. Boosting photocatalytic CO_2 reduction efficiency by heterostructures of NH_2-MIL-101(Fe)/g-C_3N_4. ACS Appl Energy Mater. 2020;3(4):3946. https://doi.org/10.1021/acsaem.0c00352.

[33] Shen Y, Han QT, Hu JQ, Gao W, Wang L, Yang LQ, Gao C, Shen Q, Wu CP, Wang XY, Zhou X, Zhou Y, Zou ZG. Artificial trees for artificial photosynthesis: Construction of dendrite-structured α-Fe_2O_3/g-C_3N_4 Z-scheme system for efficient CO_2 reduction into solar fuels. ACS Appl Energy Mater. 2020; 3(7):6561. https://doi.org/10.1021/acsaem.0c00750.

[34] Tahir M. Construction of a stable two-dimensional MAX supported protonated graphitic carbon nitride (pg-C_3N_4)/Ti_3AlC_2/TiO_2 Z-scheme multiheterojunction system for efficient photocatalytic CO_2 reduction through dry reforming of methanol. Energy Fuels. 2020;34(3):3540. https://doi.org/10.1021/acs.energyfuels.9b04393.

[35] Vu NN, Kaliaguine S, Do TO. Synthesis of the g-C_3N_4/CdS nanocomposite with a chemically bonded interface for enhanced sunlight-driven CO_2 photoreduction. ACS Appl Energy Mater. 2020;3(7):6422. https://doi.org/10.1021/acsaem.0c00656.

[36] Zhou AQ, Yang JM, Zhu XW, Zhu XL, Liu JY, Zhong K, Chen HX, Chu JY, Du YS, Song YH, Qian JC, Li HM, Xu H. Self-assembly construction of NiCo LDH/ultrathin g-C_3N_4 nanosheets photocatalyst for enhanced CO_2 reduction and charge separation mechanism study. Rare Met. 2022;41(6): 2118. https://doi.org/10.1007/s12598-022-01960-z.

[37] Zhao YX, Cai W, Shi YP, Tang JY, Gong YH, Chen MD, Zhong Q. Construction of nano-Fe_2O_3-decorated flower-like MoS_2 with Fe-S bonds for efficient photoreduction of CO_2 under visible-light irradiation. ACS Sustain Chem Eng. 2020; 8(33):12603. https://doi.org/10.1021/acssuschemeng.0c04042.

[38] Zhu Z, Liu ZX, Tang X, Reeti K, Huo PW, Wong JWC, Zhao J. Sulfur-doped g-C_3N_4 for efficient photocatalytic CO_2 reduction: insights by experiment and first-principles calculations. Catal Sci Technol. 2021;11(5):1725. https://doi.org/10.1039/d0cy02382e.

[39] Niu Q, Cheng Z, Chen QS, Huang GC, Lin JY, Bi JH, Wu L. Constructing nitrogen self-doped covalent triazine-based frameworks for visible-light-driven photocatalytic conversion of CO_2 into CH_4. ACS Sustain Chem Eng. 2021;9(3):1333. https://doi.org/10.1021/acssuschemeng.0c07930.

[40] Palazzetti F, Tsai PY. Photodissociation dynamics of CO-forming channels on the ground-state surface of methyl formate at 248 nm: direct dynamics study and assessment of generalized multicenter impulsive models. J Phys Chem A. 2021;125(5):1198. https://doi.org/10.1021/acs.jpca.0c10464.

[41] Liu JF, Wang P, Fan JJ, Yu HG, Yu JG. In situ synthesis of Mo_2C nanoparticles on graphene nanosheets for enhanced photocatalytic H_2-production activity of TiO_2. ACS Sustain Chem Eng. 2021;9(10):3828. https://doi.org/10.1021/acssuschemeng.0c08903.

[42] Ren J, Ouyang SX, Xu H, Meng XG, Wang T, Wang DF, Ye JH. Targeting activation of CO_2 and H_2 over Ru-loaded ultrathin layered double hydroxides to achieve efficient photothermal CO_2 methanation in flow-type system. Adv Energy Mater. 2017;7(5):1601657. https://doi.org/10.1002/aenm.201601657.

[43] Li SH, Qi MY, Fan YY, Yang Y, Anpo M, Yamada YMA, Tang ZR, Xu YJ. Modulating photon harvesting through dynamic non-covalent interactions for enhanced photochemical CO_2 reduction. Appl Catal B. 2021;292: 120157. https://doi.org/10.1016/j.apcatb.2021.120157.
[44] Qi MY, Lin Q, Tang ZR, Xu YJ. Photoredox coupling of benzyl alcohol oxidation with CO_2 reduction over CdS/TiO_2 heterostructure under visible light irradiation. Appl Catal B. 2022;307:121158. https://doi.org/10.1016/j.apcatb.2022.121158.
[45] Bjelajac A, Kopač D, Fecant A, Tavernier E, Petrović R, Likozar B, Janaćković D. Micro-kinetic modelling of photocatalytic CO_2 reduction over undoped and N-doped TiO_2. Catal Sci Technol. 2020;10(6):1688. https://doi.org/10.1039/c9cy02443c.
[46] Di J, Song P, Zhu C, Chen C, Xiong J, Duan ML, Long R, Zhou WQ, Xu MZ, Kang LX, Lin B, Liu DB, Chen SM, Liu CT, Li HM, Zhao YL, Li SZ, Yan QY, Song L, Liu Z. Strain-engineering of $Bi_{12}O_{17}Br_2$ nanotubes for boosting photocatalytic C_{O2} reduction. ACS Mater Lett. 2020;2(8):1025. https://doi.org/10.1021/acsmaterialslett.0c00306.
[47] Guo SH, Qi XJ, Zhou HM, Zhou J, Wang XH, Dong M, Zhao X, Sun CY, Wang XL, Su ZM. A bimetallic-MOF catalyst for efficient CO_2 photoreduction from simulated flue gas to value-added formate. J Mater Chem A. 2020;8(23):11712. https://doi.org/10.1039/d0ta00205d.
[48] He JH, Lv P, Zhu J, Li HX. Selective CO_2 reduction to HCOOH on a $Pt/In_2O_3/g\text{-}C_3N_4$ multifunctional visible-photocatalyst. RSC Adv. 2020;10(38):22460. https://doi.org/10.1039/d0ra03959d.
[49] Kumar N, Kumar S, Gusain R, Manyala N, Eslava S, Ray SS. Polypyrrole-promoted rGO–MoS_2 nanocomposites for enhanced photocatalytic conversion of CO_2 and H_2O to CO, CH_4, and H_2 products. ACS Appl Energy Mater. 2020;3(10):9897. https://doi.org/10.1021/acsaem.0c01602.
[50] Lee S, Kim S, Park C, Moon Gh, Son HJ, Baeg JO, Kim W, Choi W. Nafion-assisted noncovalent assembly of molecular sensitizers and catalysts for sustained photoreduction of CO_2 to CO. ACS Sustain Chem Eng. 2020;8(9):3709. https://doi.org/10.1021/acssuschemeng.9b06797.
[51] Li J, Liu P, Huang HL, Li Y, Tang YZ, Mei DH, Zhong CL. Metal-free 2D/2D black phosphorus and covalent triazine framework heterostructure for CO_2 photoreduction. ACS Sustain Chem Eng. 2020;8(13):5175. https://doi.org/10.1021/acssuschemeng.9b07591.
[52] Liu J, Liu M, Yang XL, Chen H, Liu SZF, Yan JQ. Photo-redeposition synthesis of bimetal Pt–Cu co-catalysts for TiO_2 photocatalytic solar-fuel production. ACS Sustain Chem Eng. 2020;8(15):6055. https://doi.org/10.1021/acssuschemeng.0c00969.
[53] Liu Q, Chen ZX, Tao WJ, Zhu HM, Zhong LX, Wang FX, Zou R, Lei YQ, Liu C, Peng XW. Edge activation of an inert polymeric carbon nitride matrix with boosted absorption kinetics and near-infrared response for efficient photocatalytic CO_2 reduction. J Mater Chem A. 2020;8(23):11761. https://doi.org/10.1039/d0ta03870a.
[54] Zhang L, Zhang LJ, Chen YM, Zheng YK, Guo J, Wan SL, Wang S, Ngaw CK, Lin JD, Wang Y. CdS/ZnO: a multipronged approach for efficient reduction of carbon dioxide under visible light irradiation. ACS Sustain Chem Eng. 2020;8(13):5270. https://doi.org/10.1021/acssuschemeng.0c00190.
[55] Bhattacharyya K, Mane GP, Rane V, Tripathi AK, Tyagi AK. Selective CO_2 photoreduction with Cu-doped TiO_2 photocatalyst: delineating the crucial role of Cu-oxidation state and oxygen vacancies. J Phys Chem C. 2021;125(3):1793. https://doi.org/10.1021/acs.jpcc.0c08441.
[56] Fu ZW, Vogel A, Zwijnenburg MA, Cooper AI, Sprick RS. Photocatalytic syngas production using conjugated organic polymers. J Mater Chem A. 2021;9(7):4291. https://doi.org/10.1039/d0ta09613j.
[57] Shao BY, Wang JY, Zhang YZ, Tan X, Zhou W, Chen YL, Xie T, Yu T. Construction of a 3D/2D $g\text{-}C_3N_4/ZnIn_2S_4$ hollow spherical heterostructure for efficient CO_2 photoreduction under visible light. Catal Sci Technol. 2021;11(4):1282. https://doi.org/10.1039/d0cy01890b.
[58] Shyamal S, Pradhan N. Halide perovskite nanocrystals photocatalysts for CO_2 reduction: success and challenges. J Phys Chem Lett. 2020;11(16):6921. https://doi.org/10.1021/acs.jpclett.0c00191.
[59] Luévano-Hipólito E, Torres-Martínez LM, Fernández-Trujillo A. Ternary ZnO/CuO/Zeolite composite obtained from volcanic ash for photocatalytic CO_2 reduction and H_2O decomposition. J Phys Chem Solids. 2021;151:109917. https://doi.org/10.1016/j.jpcs.2020.109917.
[60] Rej S, Bisetto M, Naldoni A, Fornasiero P. Well-defined Cu_2O photocatalysts for solar fuels and chemicals. J Mater Chem A. 2021;9(10):5915. https://doi.org/10.1039/d0ta10181h.
[61] Shi L, Ren XH, Wang Q, Zhou W, Ye JH. Tridecaboron diphosphide: a new infrared light active photocatalyst for efficient CO_2 photoreduction under mild reaction conditions. J Mater Chem A. 2021;9(4):2421. https://doi.org/10.1039/d0ta10804a.
[62] Zhu ZJ, Hu X, An XD, Xiao MQ, Zhang L, Li CR, He L. Photothermal catalytic CO_2 hydrogenation with high activity and tailored selectivity over monodispersed Pd-Ni nanoalloys. Chem-An Asian J. 2022;17(24):202200993. https://doi.org/10.1002/asia.202200993.
[63] Hu YG, Zhan F, Wang Q, Sun YJ, Yu C, Zhao X, Wang H, Long R, Zhang GZ, Gao C, Zhang WK, Jiang J, Tao Y, Xiong YJ. Tracking mechanistic pathway of photocatalytic CO_2 reaction at Ni sites using operando, time-resolved spectroscopy. J Am Chem Soc. 2020;142(12):5618. https://doi.org/10.1021/jacs.9b12443.
[64] Jiang LX, Li XN, He SG. Metal-dependent selectivity on the reactions of carbon dioxide with diatomic hydride anions MH– (M = Co, Ni, and Cu). J Phys Chem C. 2020;124(11):5928. https://doi.org/10.1021/acs.jpcc.9b11619.
[65] Jones WD. Carbon capture and conversion. J Am Chem Soc. 2020;142(11):4955. https://doi.org/10.1021/jacs.0c02356.
[66] Singh D, Gupta SK, Seriani N, Lukačević I, Sonvane Y, Gajjar PN, Ahuja R. Mechanism of formaldehyde and formic acid formation on $(101)\text{-}TiO_2@Cu_4$ systems through CO_2 hydrogenation. Sustain Energy Fuels. 2021;5(2):564. https://doi.org/10.1039/d0se01587c.
[67] Yuan L, Qi MY, Tang ZR, Xu YJ. Coupling strategy for CO_2 valorization integrated with organic synthesis by heterogeneous photocatalysis. Angew Chem Int Ed. 2021;60(39):21150. https://doi.org/10.1002/anie.202101667.
[68] Meng XG, Liu LQ, Ouyang SX, Xu H, Wang DF, Zhao NQ, Ye JH. Nanometals for solar-to-chemical energy conversion: from semiconductor-based photocatalysis to plasmon-mediated photocatalysis and photo-thermocatalysis. Adv Mater. 2016;28(32):6781. https://doi.org/10.1002/adma.201600305.
[69] Han C, Li YH, Li JY, Qi MY, Tang ZR, Xu YJ. Cooperative syngas production and C-N bond formation in one photoredox cycle. Angew Chem Int. 2021;60(14):7962. https://doi.org/10.1002/anie.202015756.
[70] Li S, Yang LJ, Ola O, Maroto-Valer M, Du XZ, Yang YP. Photocatalytic reduction of CO_2 by CO co-feed combined with photocatalytic water splitting in a novel twin reactor. Energy Convers Manage. 2016;116:184. https://doi.org/10.1016/j.enconman.2016.03.001.

[71] Zhang J, Lv S, Zheng JL, Yang PL, Li J, Wu XH, Jin TX, Cheng CX, Song YW, Li L. Self-CO_2 recycling photocatalytic fuel cell for enhancing degradation of pollutants and production of carbon-neutral fuel. ACS Sustain Chem Eng. 2020;8(30):11133. https://doi.org/10.1021/acssuschemeng.0c01906.

[72] Guene Lougou B, Hong JR, Shuai Y, Huang X, Yuan Y, Tan HP. Production mechanism analysis of H_2 and CO via solar thermochemical cycles based on iron oxide (Fe_3O_4) at high temperature. Sol Energy. 2017;148:117. https://doi.org/10.1016/j.solener.2017.03.050.

[73] Shuai Y, Guene Lougou B, Zhang H, Zhao JP, Ahouannou C, Tan HP. Heat transfer analysis of solar-driven high-temperature thermochemical reactor using NiFe-aluminate RPCs. Int J Hydrogen Energy. 2021;46(16):10104. https://doi.org/10.1016/j.ijhydene.2020.03.240.

[74] Giret Y, Guo P, Wang LF, Cheng J. Theoretical study of kinetics of proton coupled electron transfer in photocatalysis. J Chem Phys. 2020;152(12):124705. https://doi.org/10.1063/5.0001825.

[75] Kočí K, Reli M, Kozák O, Lacný Z, Plachá D, Praus P, Obalová L. Influence of reactor geometry on the yield of CO_2 photocatalytic reduction. Catal Today. 2011;176(1):212. https://doi.org/10.1016/j.cattod.2010.12.054.

[76] Kron KJ, Gomez SJ, Mao YZ, Cave RJ, Mallikarjun SS. Computational analysis of electron transfer kinetics for CO_2 reduction with organic photoredox catalysts. J Phys Chem A. 2020;124(26):5359. https://doi.org/10.1021/acs.jpca.0c03065.

[77] Thompson WA, Sanchez Fernandez E, Maroto-Valer MM. Review and analysis of CO_2 photoreduction kinetics. ACS Sustain Chem Eng. 2020;8(12):4677. https://doi.org/10.1021/acssuschemeng.9b06170.

[78] Prusty D, Paramanik L, Parida K. Recent advances on alloyed quantum dots for photocatalytic hydrogen evolution: a mini-review. Energy Fuels. 2021;35(6):4670. https://doi.org/10.1021/acs.energyfuels.0c04163.

[79] Ashrafi H, Akhond M, Zare M, Absalan G. Characterizing carbon ring-C_3N_4 nanosheets as a light-harvesting and charge carrier transfer agent: photodegradation of methylene blue and photoconversion of CO_2 to CH_4 as case studies. Ind Eng Chem Res. 2021;60(10):3893. https://doi.org/10.1021/acs.iecr.0c05626.

[80] Bian J, Sun L, Zhang ZQ, Li ZJ, Chu MN, Li X, Tang DY, Jing LQ. Au-modulated Z-scheme CuPc/$BiVO_4$ nanosheet heterojunctions toward efficient CO_2 conversion under wide-visible-light irradiation. ACS Sustain Chem Eng. 2021;9(5):2400. https://doi.org/10.1021/acssuschemeng.0c09256.

[81] Qiu QQ, Zhu P, Liu Y, Liang TX, Xie TF, Lin YH. Highly efficient In_2S_3/WO_3 photocatalysts: Z-scheme photocatalytic mechanism for enhanced photocatalytic water pollutant degradation under visible light irradiation. RSC Adv. 2021;11(6):3333. https://doi.org/10.1039/d0ra09315g.

[82] Jin XL, Xu YX, Zhou X, Lv CD, Huang QZ, Chen G, Xie HQ, Ge T, Cao J, Zhan JQ, Ye LQ. Single-atom Fe triggers superb CO_2 photoreduction on a bismuth-rich catalyst. ACS Mater Lett. 2021;3(4):364. https://doi.org/10.1021/acsmaterialslett.1c00091.

[83] Zhao ZY, Liu W, Shi YT, Zhang HM, Song XD, Shang WZ, Hao C. An insight into the reaction mechanism of CO_2 photoreduction catalyzed by atomically dispersed Fe atoms supported on graphitic carbon nitride. Phys Chem Chem Phys. 2021;23(8):4690. https://doi.org/10.1039/d0cp05570k.

[84] Zhang XD, Kim D, Lee LYS. Copper-doped ZnS with internal phase junctions for highly selective CO production from CO_2 photoreduction. ACS Appl Energy Mater. 2021;4(3):2586. https://doi.org/10.1021/acsaem.0c03163.

[85] Wang GY, Chen WQ, Zhang Y, Xu QS, Li YR, Foo ML, Tang L. Synthesis of $ZnIn_2S_4$@Co_3S_4 particles derived from ZIF-67 for photocatalytic hydrogen production. RSC Adv. 2021;11(16):9296. https://doi.org/10.1039/d0ra10799a.

[86] Bhatta S, Nagassou D, Mohsenian S, Trelles JP. Photo-thermochemical decomposition of carbon-dioxide in a direct solar receiver-reactor. Sol Energy. 2019;178:201. https://doi.org/10.1016/j.solener.2018.12.019.

[87] Ullah S, Lovell EC, Wong RJ, Tan TH, Scott J, Amal R. Light-enhanced CO_2 reduction to CH_4 using nonprecious transition-metal catalysts. ACS Sustain Chem Eng. 2020;8(13):5056. https://doi.org/10.1021/acssuschemeng.9b06823.

[88] Vagia EC, Muradov N, Kalyva A, Raissi TA, Qin N, Srinivasa AR, Kakosimos KE. Solar hybrid photo-thermochemical sulfur-ammonia water-splitting cycle: photocatalytic hydrogen production stage. Int J Hydrogen Energy. 2017;42(32):20608. https://doi.org/10.1016/j.ijhydene.2017.06.210.

[89] Wang CL, Fang SY, Xie SH, Zheng Y, Hu YH. Thermo-photo catalytic CO_2 hydrogenation over Ru/TiO_2. J Mater Chem A. 2020;8(15):7390. https://doi.org/10.1039/c9ta13275a.

[90] Li YZ, Wu SW, Wu JC, Hu QQ, Zhou CY. Photothermocatalysis for efficient abatement of CO and VOCs. J Mater Chem A. 2020;8(17):8171. https://doi.org/10.1039/d0ta00029a.

[91] Snoeckx R, Bogaerts A. Plasma technology—a novel solution for CO_2 conversion? Chem Soc Rev. 2017;46(19):5805. https://doi.org/10.1039/c6cs00066e.

[92] Zhu LL, Gao MM, Peh CKN, Ho GW. Solar-driven photothermal nanostructured materials designs and prerequisites for evaporation and catalysis applications. Mater Horiz. 2018;5(3):323. https://doi.org/10.1039/c7mh01064h.

[93] Liu HM, Shi LZ, Zhang QJ, Qi P, Zhao YH, Meng QR, Feng XQ, Wang H, Ye JH. Photothermal catalysts for hydrogenation reactions. Chem Commun. 2021;57(11):1279. https://doi.org/10.1039/d0cc07144g.

[94] Bhatta S, Nagassou D, Trelles JP. Solar photo-thermochemical reactor design for carbon dioxide processing. Sol Energy. 2017;142:253. https://doi.org/10.1016/j.solener.2016.12.031.

[95] Tang SL, Sun J, Hong H, Liu QB. Solar fuel from photo-thermal catalytic reactions with spectrum-selectivity: a review. Front Energy. 2017;11(4):437. https://doi.org/10.1007/s11708-017-0509-z.

[96] Poudyal S, Laursen S. Insights into elevated-temperature photocatalytic reduction of CO_2 by H_2O. J Phys Chem C. 2018;122(15):8045. https://doi.org/10.1021/acs.jpcc.7b12662.

[97] Vaiano V, Sannino D, Ciambelli P. Steam reduction of CO_2 on Pd/TiO_2 catalysts: a comparison between thermal and photocatalytic reactions. Photochem Photobiol Sci. 2015;14(3):550. https://doi.org/10.1039/c4pp00252k.

[98] Liang HX, Wang FQ, Cheng ZM, Hu SP, Xiao B, Gong XT, Lin B, Tan JY, Li XZ, Cao RY, Liang W, Lin LH. Analyzing the effects of reaction temperature on photo-thermo chemical synergetic catalytic water splitting under full-spectrum solar irradiation: An experimental and thermodynamic investigation. Int J Hydrogen Energy. 2017;42(17):12133. https://doi.org/10.1016/j.ijhydene.2017.03.194.

[99] Upadhye AA, Ro I, Zeng X, Kim HJ, Tejedor I, Anderson MA, Dumesic JA, Huber GW. Plasmon-enhanced reverse water gas shift reaction over oxide supported Au catalysts. Catal Sci Technol. 2015;5(5):2590. https://doi.org/10.1039/c4cy01183j.

[100] Fang J, Liu QB, Guo SP, Lei J, Jin HG. Spanning solar spectrum: a combined photochemical and thermochemical process for solar energy storage. Appl Energy. 2019;247:116. https://doi.org/10.1016/j.apenergy.2019.04.043.

[101] Fu MK, Wang L, Ma TZ, Ma HT, Xu HJ, Li X. Mechanism of CO production around oxygen vacancy of $LaMnO_3$: an efficient and rapid evaluation of the doping effect on the kinetics

and thermodynamic driving force of CO_2-splitting. J Mater Chem A. 2020;8(4):1709. https://doi.org/10.1039/c9ta09764c.
[102] Dias Vicentini E, de Lima Batista AP, Sampaio de Oliveir-a-Filho AG. Computational mechanistic investigation of the Fe + CO2→ FeO + CO reaction. Phys Chem Phys. 2020;22(29): 16943. https://doi.org/10.1039/d0cp00479k.
[103] Shuai Y, Guene Lougou B, Zhang H, Han DM, Jiang BS, Zhao JP, Huang X. Combined heat and mass transfer analysis of solar reactor integrating porous reacting media for water and carbon dioxide splitting. Sol Energy. 2022;242:130. https://doi.org/10.1016/j.solener.2022.07.017.
[104] Guene Lougou B, Geng BX, Jiang BS, Zhang H, Sun QM, Shuai Y, Qu ZB, Zhao JP, Wang CH. Copper ferrite and cobalt oxide two-layer coated macroporous SiC substrate for efficient CO_2-splitting and thermochemical energy conversion. J Colloid Interface Sci. 2022;627:516. https://doi.org/10.1016/j.jcis.2022.07.057.
[105] Fang J, Liu QB, Guo SP, Lei J. A full-spectrum solar chemical energy storage system with photochemical process and thermochemical process. Energy Procedia. 2018;152:1063. https://doi.org/10.1016/j.egypro.2018.09.120.
[106] Jia J, O'Brien PG, He L, Qiao Q, Fei T, Reyes LM, Burrow TE, Dong YC, Liao K, Varela M, Pennycook SJ, Hmadeh M, Helmy AS, Kherani NP, Perovic DD, Ozin GA. Visible and near-infrared photothermal catalyzed hydrogenation of gaseous CO_2 over nanostructured Pd@Nb_2O_5. Adv Sci. 2016;3(10): 1600189. https://doi.org/10.1002/advs.201600189.
[107] Zhu Q, Ye K, Zhu W, Xu WJ, Zou CW, Song L, Sharman E, Wang LJ, Jin SY, Zhang GZ, Luo Y, Jiang J. A hydrogenated metal oxide with full solar spectrum absorption for highly efficient photothermal water evaporation. J Phys Chem Lett. 2020;11(7):2502. https://doi.org/10.1021/acs.jpclett.0c00592.
[108] Li ZX, Gong YX, Zhang X, Wen YY, Yao JS, Hu ML, He M, Liu JH, Li R, Wang FQ, Zhang CX. Plasmonic coupling-enhanced in situ photothermal nanoreactor with shape selective catalysis for C-C coupling reaction. Nano Res. 2020;13:2812. https://doi.org/10.1007/s12274-020-2933-3.
[109] Wang LC, Wang Y, Cheng Y, Liu ZF, Guo QS, Ha MN, Zhao Z. Hydrogen-treated mesoporous WO_3 as a reducing agent of CO_2 to fuels (CH_4 and CH_3OH) with enhanced photothermal catalytic performance. J Mater Chem A. 2016;4(14):5314. https://doi.org/10.1039/c5ta10180h.
[110] Ren L, Li YZ, Liu HH, Mao MY, Lan L, Zhao XJ. UV–Vis-infrared light-driven photothermocatalytic synergetic effect leading to efficient benzene abatement by Pt supported on anatase TiO_2 with 001 facets. ACS Appl Energy Mater. 2020;3(8):7920. https://doi.org/10.1021/acsaem.0c01310.
[111] Schwartzenberg KC, Hamilton JWJ, Lucid AK, Weitz E, Notestein J, Nolan M, Byrne JA, Gray KA. Multifunctional photo/thermal catalysts for the reduction of carbon dioxide. Catal Today. 2017;280:65. https://doi.org/10.1016/j.cattod.2016.06.002.
[112] Tang HB, Tang ZH, Bright J, Liu BT, Wang XJ, Meng GW, Wu NQ. Visible-light localized surface plasmon resonance of WO_{3-x} nanosheets and its photocatalysis driven by plasmonic hot carriers. ACS Sustain Chem Eng. 2021;9(4):1500. https://doi.org/10.1021/acssuschemeng.0c08140.
[113] Liu HM, Dao TD, Liu LQ, Meng XG, Nagao T, Ye JH. Light assisted CO_2 reduction with methane over group VIII metals: universality of metal localized surface plasmon resonance in reactant activation. Appl Catal B. 2017;209:183. https://doi.org/10.1016/j.apcatb.2017.02.080.
[114] Zhang XG, Zhang L, Feng SS, Qin HM, Wu DY, Zhao Y. Light driven mechanism of carbon dioxide reduction reaction to carbon monoxide on gold nanoparticles: a theoretical prediction. J Phys Chem Lett. 2021;12(4):1125. https://doi.org/10.1021/acs.jpclett.0c03694.
[115] Wang L, Liu XX, Dang YL, Xie HG, Zhao Q, Ye LQ. Enhanced solar induced photo-thermal synergistic catalytic CO_2 conversion by photothermal material decorated TiO_2. Solid State Sci. 2019;89:67. https://doi.org/10.1016/j.solidstatesciences.2018.12.018.
[116] Chen LY, Huang KL, Xie QR, Lam SM, Sin JC, Su TM, Ji HB, Qin ZZ. The enhancement of photocatalytic CO_2 reduction by the in situ growth of TiO_2 on Ti_3C_2 Mxene. Catal Sci Technol. 2021;11(4):1602. https://doi.org/10.1039/D0CY02212H.
[117] Mateo D, Cerrillo JL, Durini S, Gascon J. Fundamentals and applications of photo-thermal catalysis. Chem Soc Rev. 2021; 50(3):2173. https://doi.org/10.1039/d0cs00357c.
[118] Kim C, Hyeon S, Lee J, Kim WD, Lee DC, Kim J, Lee H. Energy-efficient CO_2 hydrogenation with fast response using photoexcitation of CO_2 adsorbed on metal catalysts. Nat Commun. 2018;9(1):3027. https://doi.org/10.1038/s41467-018-05542-5.
[119] Li YG, Hao JC, Song H, Zhang FY, Bai XH, Meng XG, Zhang HY, Wang SF, Hu Y, Ye JH. Selective light absorber-assisted single nickel atom catalysts for ambient sunlight-driven CO_2 methanation. Nat Commun. 2019;10(1):2359. https://doi.org/10.1038/s41467-019-10304-y.
[120] Westrich TA, Dahlberg KA, Kaviany M, Schwank JW. High-temperature photocatalytic ethylene oxidation over TiO_2. J Phys Chem C. 2011;115(33):16537. https://doi.org/10.1021/jp204405h.
[121] Zheng YK, Zhang L, Guan J, Qian SY, Zhang ZX, Ngaw CK, Wan SL, Wang S, Lin JD, Wang Y. Controlled synthesis of Cu0/Cu_2O for efficient photothermal catalytic conversion of CO_2 and H_2O. ACS Sustain Chem Eng. 2021;9(4):1754. https://doi.org/10.1021/acssuschemeng.0c07702.
[122] Sastre F, Versluis C, Meulendijks N, Rodriguez-Fernandez J, Sweelssen J, Elen K, Van Bael MK, Den Hartog T, Verheijen MA, Buskens P. Sunlight-fueled, low-temperature Ru-catalyzed conversion of CO_2 and H_2 to CH_4 with a high photon-to-methane efficiency. ACS Omega. 2019;4(4):7369. https://doi.org/10.1021/acsomega.9b00581.
[123] Meng XG, Wang T, Liu LQ, Ouyang SX, Li P, Hu HL, Kako T, Iwai H, Tanaka A, Ye JH. Photothermal conversion of CO_2 into CH_4 with H_2 over group VIII nanocatalysts: an alternative approach for solar fuel production. Angew Chem Int Ed. 2014; 53(43):11478. https://doi.org/10.1002/anie.201404953.
[124] Jantarang S, Lovell EC, Tan TH, Scott J, Amal R. Role of support in photothermal carbon dioxide hydrogenation catalysed by Ni/$Ce_xTi_yO_2$. Progr Nat Sci: Mater Int. 2018;28(2):168. https://doi.org/10.1016/j.pnsc.2018.02.004.
[125] Cao XE, Kaminer Y, Hong T, Schein P, Liu T, Hanrath T, Erickson D. HI-Light: a glass-waveguide-based "shell-and--tube" photothermal reactor platform for converting CO_2 to fuels. Iscience. 2020. https://doi.org/10.1016/j.isci.2020.101856.
[126] Novoa-Cid M, Baldovi HG. Study of the photothermal catalytic mechanism of CO_2 reduction to CH_4 by ruthenium nanoparticles supported on titanate nanotubes. Nanomaterials. 2020;10(11):2212. https://doi.org/10.3390/nano10112212.
[127] Zhao JQ, Yang Q, Shi R, Waterhouse GIN, Zhang X, Wu LZ, Tung CH, Zhang TR. FeO–CeO_2 nanocomposites: an efficient and highly selective catalyst system for photothermal CO_2 reduction to CO. NPG Asia Mater. 2020;12(1):5. https://doi.org/10.1038/s41427-019-0171-5.
[128] Jiang BS, Guene Lougou B, Zhang H, Geng BX, Wu LX, Shuai Y. Preparation and solar thermochemical properties analysis of $NiFe_2O_4$@SiC/ @Si_3N_4 for high-performance CO_2-splitting.

Appl Energy. 2022;328:120057. https://doi.org/10.1016/j.apenergy.2022.120057.
[129] Gao MM, Connor PKN, Ho GW. Plasmonic photothermic directed broadband sunlight harnessing for seawater catalysis and desalination. Energy Environ Sci. 2016;9(10):3151. https://doi.org/10.1039/c6ee00971a.
[130] Song R, Luo B, Jing DW. Efficient photothermal catalytic hydrogen production over nonplasmonic Pt metal supported on TiO_2. Solar Hydrogen Nanotechnol XI. 2016;9935:99350C. https://doi.org/10.1117/12.2239178.
[131] Guene Lougou B, Wu LX, Ma DN, Geng BX, Jiang BS, Han DM, Zhang H, Łapka P, Shuai Y. Efficient conversion of solar energy through a macroporous ceramic receiver coupling heat transfer and thermochemical reactions. Energy. 2023;271:126989. https://doi.org/10.1016/j.energy.2023.126989.
[132] Wu LX, Guene Lougou B, Jiang BS, Zhang H, Guo YM, Geng BX, Yan TT, Łapka P, Shuai Y. Experimentally validated numerical model of multi-spectral bands radiative transport in solar receiver/reactor with photo-active porous absorber reacting media. Energy Convers Manage. 2023;278:116740. https://doi.org/10.1016/j.enconman.2023.116740.
[133] Guene Lougou B, Han DM, Zhang H, Jiang BS, Anees J, Ahouannou C, Zhao JP, Shuai Y. Numerical and experimental analysis of reactor optimum design and solar thermal-chemical energy conversion for multidisciplinary applications. Energy Convers Manage. 2020;213:112870. https://doi.org/10.1016/j.enconman.2020.112870.
[134] Kho ET, Tan TH, Lovell E, Wong RJ, Scott J, Amal R. A review on photo-thermal catalytic conversion of carbon dioxide. Green Energy Environ. 2017;2(3):204. https://doi.org/10.1016/j.gee.2017.06.003.
[135] Iglesias-Juez A, Coronado JM. Light and heat joining forces: methanol from photothermal CO_2 hydrogenation. Chem. 2018;4(7):1490. https://doi.org/10.1016/j.chempr.2018.06.015.
[136] Lou ZR, Yuan DC, Zhang FY, Wang YC, Li YG, Zhu LP. Fe_3Si assisted Co_3O_4 nanorods: a case study of photothermal catalytic CO oxidation under ambient solar irradiation. Nano Energy. 2019;62:653. https://doi.org/10.1016/j.nanoen.2019.05.080.
[137] Tang SL, Xing XL, Yu W, Sun J, Xuan YM, Wang L, Xu YF, Hong H, Jin HG. Synergizing photo-thermal H_2 and photovoltaics into a concentrated sunlight use. iScience. 2020;23(4):101012. https://doi.org/10.1016/j.isci.2020.101012.
[138] Reed NL, Yoon TP. Oxidase reactions in photoredox catalysis. Chem Soc Rev. 2021;50(5):2954. https://doi.org/10.1039/d0cs00797h.
[139] Steeves TM, Esser-Kahn AP. Demonstration of the photothermal catalysis of the Sabatier reaction using nickel nanoparticles and solar spectrum light. RSC Adv. 2021;11(14):8394. https://doi.org/10.1039/d0ra09939b.
[140] Zhang H, Zhang XM, Yang DZ, Shuai Y, Guene Lougou B, Pan QH, Wang FQ. Selection of iron-based oxygen carriers for two-step solar thermochemical splitting of carbon dioxide. Energy Convers Manage. 2023;279:116772. https://doi.org/10.1016/j.enconman.2023.116772.
[141] Li HJ, Chi HY, Hu S, He LM, Xu K, Mostafa ME, El-Sayed SA, Wang Y, Su S, Xiang J. Combustion behavior of large size coal over a wide range of heating rates in a concentrating photothermal reactor. Fuel Process Technol. 2020;197:106187. https://doi.org/10.1016/j.fuproc.2019.106187.
[142] Mohsenian S, Nagassou D, Bhatta S, Elahi R, Trelles JP. Design and characterization of a solar-enhanced microwave plasma reactor for atmospheric pressure carbon dioxide decomposition. Plasma Sources Sci Technol. 2019;28(6):065001. https://doi.org/10.1088/1361-6595/ab1c43.
[143] Li ZH, Liu JJ, Zhao YF, Shi R, Waterhouse GIN, Wang YS, Wu LZ, Tung CH, Zhang TR. Photothermal hydrocarbon synthesis using alumina-supported cobalt metal nanoparticle catalysts derived from layered-double-hydroxide nanosheets. Nano Energy. 2019;60:467. https://doi.org/10.1016/j.nanoen.2019.03.069.
[144] Chen Y, Zhang YM, Fan GZ, Song LZ, Jia G, Huang HT, Ouyang SX, Ye JH, Li ZS, Zou ZG. Cooperative catalysis coupling photo-/photothermal effect to drive Sabatier reaction with unprecedented conversion and selectivity. Joule. 2021;5(12):3235. https://doi.org/10.1016/j.joule.2021.11.009.
[145] Wu ZY, Shen JH, Li CR, Zhang CC, Feng K, Wang ZQ, Wang XC, Meira DM, Cai MJ, Zhang DK, Wang SH, Chu MY, Chen JX, Xi YY, Zhang L, Sham TK, Genest A, Rupprechter G, Zhang XH, He L. Mo_2TiC_2 MXene-supported Ru clusters for efficient photothermal reverse water-gas shift. ACS Nano. 2022;17(2):1550. https://doi.org/10.1021/acsnano.2c10707.
[146] Shen JH, Tang R, Wu ZY, Wang X, Chu MY, Cai MJ, Zhang CC, Zhang L, Yin K, He L, Li CR. Integrated photothermal nanoreactors for efficient hydrogenation of CO_2. Transact Tianjin Univ. 2022;28(4):236. https://doi.org/10.1007/s12209-022-00333-y.
[147] Huang WX, Li ZP, Li DD, Hu ZH, Wu C, Lv KL, Li Q. Ti_3C_2 MXene: recent progress in its fundamentals, synthesis, and applications. Rare Met. 2022;41(10):3268. https://doi.org/10.1007/s12598-022-02058-2.
[148] Wang L, Dong YC, Yan TJ, Hu ZX, Ali FM, Meira DM, Duchesne PN, Loh JYY, Qiu CY, Storey EE, Xu YF, Sun W, Ghoussoub M, Kherani NP, Helmy AS, Ozin GA. Black indium oxide a photothermal CO_2 hydrogenation catalyst. Nat Commun. 2020;11(1):2432. https://doi.org/10.1038/s41467-020-16336-z.
[149] Ghoussoub M, Xia MK, Duchesne PN, Segal D, Ozin G. Principles of photothermal gas-phase heterogeneous CO_2 catalysis. Energy Environ Sci. 2019;12(4):1122. https://doi.org/10.1039/c8ee02790k.
[150] Cai MJ, Wu ZY, Li Z, Wang L, Sun W, Tountas AA, Li CR, Wang SH, Feng K, Xu AB, Tang SL, Tavasoli A, Peng MW, Liu WX, Helmy AS, He L, Ozin GA, Zhang XH. Greenhouse-inspired supra-photothermal CO_2 catalysis. Nat Energy. 2021;6(8):807. https://doi.org/10.1038/s41560-021-00867-w.
[151] Cai MJ, Li CR, He L. Enhancing photothermal CO_2 catalysis by thermal insulating substrates. Rare Met. 2020;39(8):881. https://doi.org/10.1007/s12598-020-01431-3.
[152] Feng K, Wang SH, Zhang DK, Wang L, Yu YY, Feng K, Li Z, Zhu ZJ, Li CR, Cai MJ, Wu ZY, Kong N, Yan BH, Zhong J, Zhang XH, Ozin GA, He L. Cobalt plasmonic superstructures enable almost 100% broadband photon efficient CO_2 photocatalysis. Adv Mater. 2020;32(24):2000014. https://doi.org/10.1002/adma.202000014.
[153] Li YG, Bai XH, Yuan DC, Yu CY, San XY, Guo YN, Zhang LQ, Ye JH. Cu-based high-entropy two-dimensional oxide as stable and active photothermal catalyst. Nat Commun. 2023;14(1):3171. https://doi.org/10.1038/s41467-023-38889-5.
[154] Jia J, Wang H, Lu ZL, O'Brien PG, Ghoussoub M, Duchesne P, Zheng ZQ, Li PC, Qiao Q, Wang L, Gu A, Ali FM, Dong YC, Wang Q, Ghuman KK, Wood T, Qian CX, Shao Y, Qiu CY, Ye MM, Zhu YM, Lu ZH, Zhang P, Helmy AS, Singh CV, Kherani NP, Perovic DD, Ozin GA. Photothermal catalyst engineering: hydrogenation of gaseous CO_2 with high activity and tailored selectivity. Adv Sci. 2017;4(10):1700252. https://doi.org/10.1002/advs.201770052.
[155] Lu KQ, Li YH, Zhang F, Qi MY, Chen X, Tang ZR, Yamada YMA, Anpo M, Conte M, Xu YJ. Rationally designed transition metal hydroxide nanosheet arrays on graphene for artificial

CO_2 reduction. Nat Commun. 2020;11(1):5181. https://doi.org/10.1038/s41467-020-18944-1.
[156] Xu QJ, Jiang JW, Wang XF, Duan LY, Guo H (2023) Understanding oxygen vacant hollow structure CeO_2@In_2O_3 heterojunction to promote CO2 reduction. Rare Met. 2023; 42(6):1888. https://doi.org/10.1007/s12598-022-02244-2.
[157] Chen LJ, Liu TT, Liu SM, Cai S, Zou XX, Jiang JW, Mei ZY, Zhao GF, Yang XF, Guo H. S vacant $CuIn_5S_8$ confined in a few-layer $MoSe_2$ with interlayer-expanded hollow heterostructures boost photocatalytic CO_2 reduction. Rare Met. 2021;41(1):144. https://doi.org/10.1007/s12598-021-01809-x.
[158] Chen YH, Qi MY, Li YH, Tang ZR, Wang T, Gong JL, Xu YJ. Activating two-dimensional $Ti_3C_2T_x$-MXene with single-atom cobalt for efficient CO_2 photoreduction. Cell Rep Phys Sci. 2021;2(3):100371. https://doi.org/10.1016/j.xcrp.2021.100371.
[159] Huang HN, Shi R, Zhang XR, Zhao JQ, Su CL, Zhang TR. Photothermal-assisted triphase photocatalysis over a multifunctional bilayer paper. Angew Chem Int Ed. 2021;60(42): 22963. https://doi.org/10.1002/anie.202110336.
[160] Wu ZY, Li CR, Li Z, Feng K, Cai MJ, Zhang DK, Wang SH, Chu MY, Zhang CC, Shen JH, Huang Z, Xiao YL, Ozin GA, Zhang XH, He L. Niobium and titanium carbides (MXenes) as superior photothermal supports for CO_2 photocatalysis. ACS Nano. 2021;15(3):5696. https://doi.org/10.1021/acsnano.1c00990.
[161] Wu ZY, Shen JH, Li CR, Zhang CC, Wu CP, Li ZM, An XD, He L. Niche applications of MXene materials in photothermal catalysis. Chemistry. 2023;5(1):492. https://doi.org/10.3390/chemistry5010036.
[162] Wang ZJ, Song H, Liu HM, Ye JH. Coupling of solar energy and thermal energy for carbon dioxide reduction: status and prospects. Angew Chem Int Ed. 2020;59(21):8016. https://doi.org/10.1002/anie.201907443.
[163] Qi YH, Song LZ, Ouyang SX, Liang XC, Ning SB, Zhang QQ, Ye JH. Photoinduced defect engineering: enhanced photothermal catalytic performance of 2D black In_2O_{3-x} nanosheets with bifunctional oxygen vacancies. Adv Mater. 2020; 32(6):1903915. https://doi.org/10.1002/adma.201903915.
[164] Wang YS, Zhao YF, Liu JJ, Li ZH, Waterhouse GIN, Shi R, Wen XD, Zhang TR. Manganese oxide modified nickel catalysts for photothermal CO hydrogenation to light olefins. Adv Energy Mater. 2019;10(5):1902860. https://doi.org/10.1002/aenm.201902860.
[165] Wei ZY, Hu KM, Sa BS, Wu B. Pressure-induced structure, electronic, thermodynamic and mechanical properties of Ti_2AlNb orthorhombic phase by first-principles calculations. Rare Met. 2017;40(10):1. https://doi.org/10.1007/s12598-017-0915-8.
[166] Zhang F, Li YH, Qi MY, Yamada YMA, Anpo M, Tang ZR, Xu YJ. Photothermal catalytic CO_2 reduction over nanomaterials. Chem Catalysis. 2021;1(2):272. https://doi.org/10.1016/j.checat.2021.01.003.
[167] Wu HK, Zhang F, Li JY, Tang ZR, Xu YJ. Photo-driven Fischer-Tropsch synthesis. J Mater Chem A. 2020;8(46):24253. https://doi.org/10.1039/d0ta09097b.
[168] Sun CY, Zhao ZW, Liu H, Wang HQ. Core–shell nanostructure for supra-photothermal CO_2 catalysis. Rare Met. 2022;41(5): 1403. https://doi.org/10.1007/s12598-021-01906-x.
[169] Song QW, He GC, Fei HL. Photothermal catalytic conversion based on single atom catalysts: fundamentals and applications. Acta Phys Chim Sinica. 2023;39(9):2212038. https://doi.org/10.3866/pku.whxb202212038.
[170] Gao CB, Lyu FL, Yin YD. Encapsulated metal nanoparticles for catalysis. Chem Rev. 2021;121(2):834. https://doi.org/10.1021/acs.chemrev.0c00237.
[171] Guo Y, Mei S, Yuan K, Wang DJ, Liu HC, Yan CH, Zhang YW. Low-temperature CO_2 methanation over CeO_2-supported Ru single atoms, nanoclusters, and nanoparticles competitively tuned by strong metal–support interactions and H-spillover effect. ACS Catal. 2018;8(7):6203. https://doi.org/10.1021/acscatal.7b04469.
[172] Rej S, Mascaretti L, Santiago EY, Tomanec O, Kment Š, Wang ZM, Zbořil R, Fornasiero P, Govorov AO, Naldoni A. Determining plasmonic hot electrons and photothermal effects during H_2 evolution with TiN–Pt nanohybrids. ACS Catal. 2020; 10(9):5261. https://doi.org/10.1021/acscatal.0c00343.
[173] Ren L, Mao MY, Li YZ, Lan L, Zhang Z, Zhao XJ. Novel photothermocatalytic synergetic effect leads to high catalytic activity and excellent durability of anatase TiO_2 nanosheets with dominant 001 facets for benzene abatement. Appl Catal B. 2016;198:303. https://doi.org/10.1016/j.apcatb.2016.05.073.
[174] Wang F, He S, Chen H, Wang B, Zheng LR, Wei M, Evans DG, Duan X. Active site dependent reaction mechanism over Ru/CeO_2 catalyst toward CO_2 methanation. J Am Chem Soc. 2016;138(19):6298. https://doi.org/10.1021/jacs.6b02762.
[175] Zhao YF, Gao W, Li SW, Williams GR, Mahadi AH, Ma D. Solar- versus thermal-driven catalysis for energy conversion. Joule. 2019;3(4):920. https://doi.org/10.1016/j.joule.2019.03.003.